Deployable Rings

by

Tim Hutt (JE)

Fourth-year undergraduate project in
Group D, 2006/2007

I hereby declare that, except where specifically indicated, the work submitted herein is my own original work.

Signed: May 29, 2007

Contents

Chapter 1

Introduction

The strict space and weight requirements imposed when transporting satellites into space create new engineering challenges for the packaging and deployment of large surfaces such as solar arrays and Synthetic Aperture Radar (SAR) antennas. SAR systems can be mounted on aircraft or satellites and are used for a variety of civil and military tasks such as surveillance. High resolution images require large SAR antennas. Many novel techniques have been developed to support these structures, with most consisting of extending booms (see [8]) and folding panels.

An example of the requirements for a SAR antenna given in [12] is for a $5 \times 1.5\,\mathrm{m}^2$ planar array packed into a $0.6 \times 0.6 \times 0.8\,\mathrm{m}^3$ space. Several solutions currently exist for deploying space structures such as these which are described below.

1.1 Extending Booms

Many varieties of extending booms exist. For example, You at Oxford University has developed an extending pantographic boom [13]. This consists of a collapsed pantographic truss structure that can be deployed by pulling an active cable that runs through the structure (figure 1.1. This is an example of an overconstrained mechanism, as are the deployale rings described later.

Rolatube Technology Ltd. manufacture bistable metal tubes [6]. Their open section makes them torsionally flexible, and hence unsuitable for supporting SAR antennas which require a high degree of geometric consistency (figure 1.2).

Another example is the telescopic boom described in [10]. A clever screw mechanism allows the segments to be extended sequentially by a single motor.

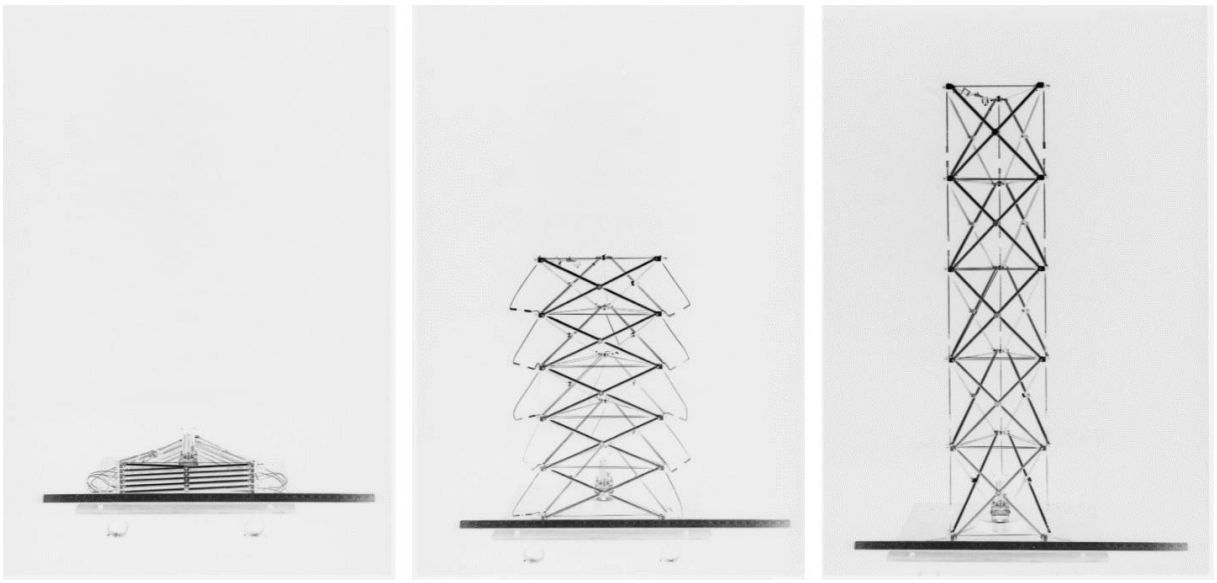

Figure 1.1: A pantographic mast developed by You. The mast is deployed by retracting a single cable that runs through the structure.

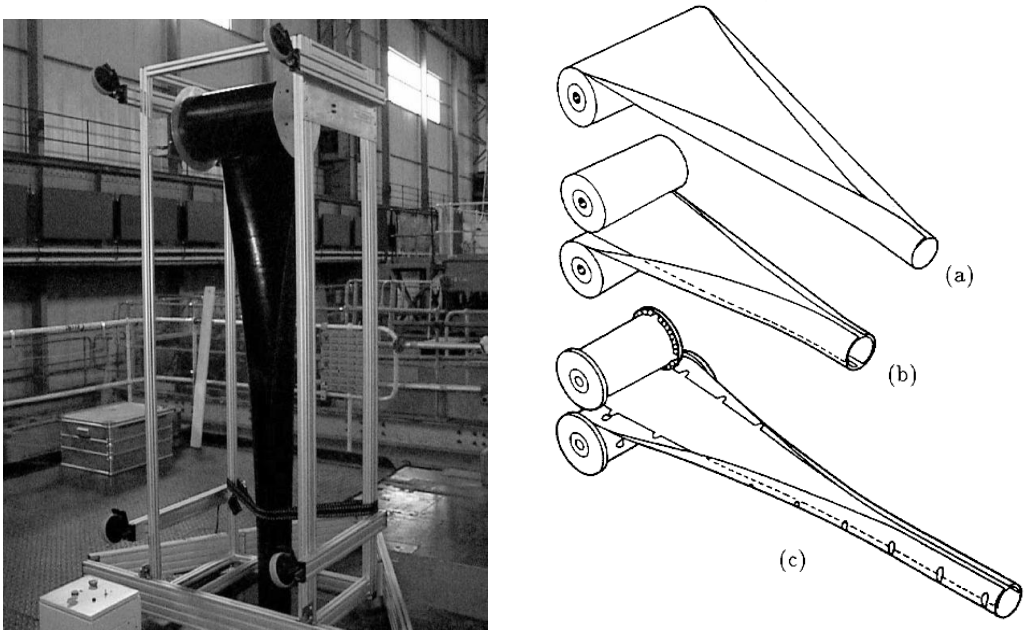

Figure 1.2: A rolatube mast (left), and a similar rolled tube design (right). The tubes are stable in the rolled up and deployed configurations.

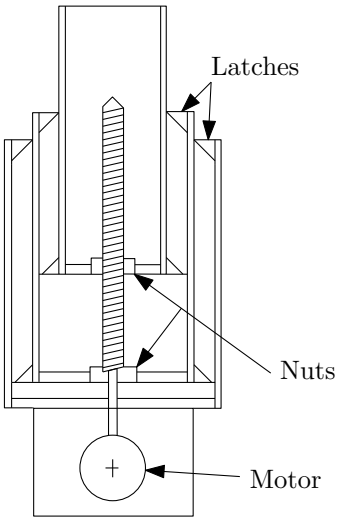

Figure 1.3: Diagram of a telescopic mast. The segments are extended by turning the screw. When one segment reaches the end of the screw it latches onto the next one and lifts it so that its nut engages with the bottom of the screw. Reproduced from [10].

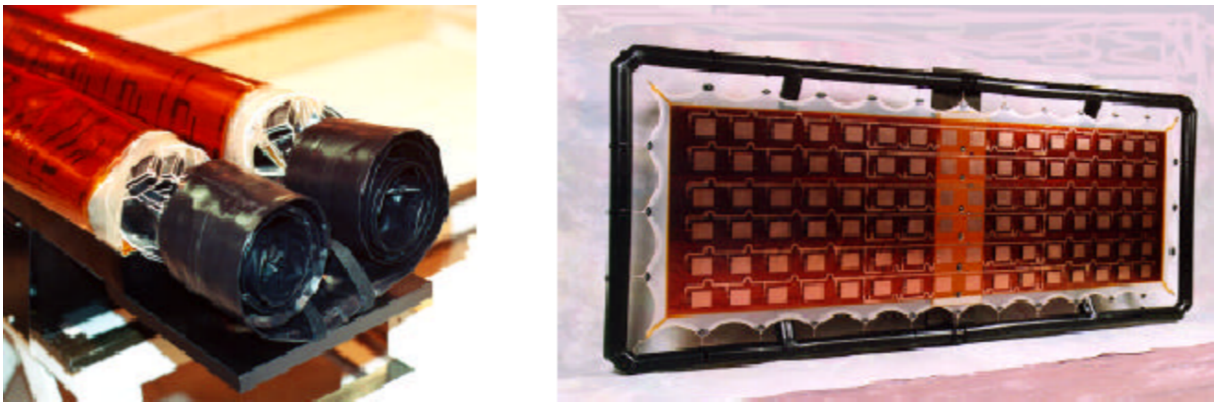

Figure 1.4: JPL's inflatable SAR frame. The antenna membrane and supports are stored rolled up (left).

1.2 Inflatable Frames

The Jet Propulsion Lab at the California Institute of Technology have developed an inflatable frame to support a SAR antenna (figure 1.4 [9]. This frame was the inspiration for the folding ring design that shall be described in this report.

1.3 Square Deployable Rings

In 1973 Hedgepeth developed a series of deployable ring mechanisms that open from a compact bundle of bars into a regular polygon [2]. The square mechanism consists of a bundle of four bars connected in a ring by single degree of freedom hinges (e.g. door hinges). It can fold out to a square as shown in figure 1.5.

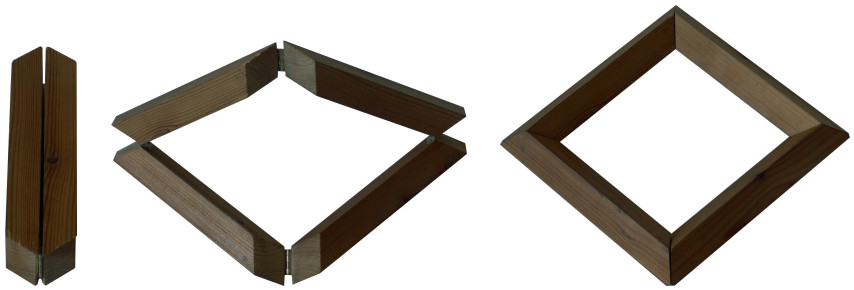

Figure 1.5: The square four-bar deployable ring.

An important feature of this mechanism is that it has a mobility of 1. This means that the mechanism can only follow a single path to deployment[1], avoiding the need for a control system or additional constraint elements.

On a satellite, a flexible or foldable membrane could be supported between the members. Pellegrino et. al have developed a lightweight hinge based on carpenters tape that provides a significant opening force, and locks rigidly when open [11]. If these were used for the hinges, deploying the mechanism involves merely releasing it. This simplicity is a major advantage over other solutions.

However, many applications require a rectangular surface rather than a square one. SAR antennas usually require an aspect ratio of at least three and often much higher. This could be provided by a chain of square rings, but a single rectangular ring would be much more elegant and efficient. Discovering and analysing such a mechanism was the purpose of this project.

[1] Assuming ideal hinges and bars, and no bifurcations in the mechanism path.

Chapter 2

The Square Four-Bar Mechanism

The properties and behaviour of the existing mechanisms were analysed before attempting to create a new one. In the following analysis it is assumed that the bars are slender and rigid, and that the hinges are perfect revolute joints. Each different frame has one or more angles that define its geometry. Altering their values gives a different frame with hinges at a different orientation. All of these angles are defined over the range $[-\pi, \pi]$. The following sections investigate the mobility condition, define the geometry of the mechanism and investigate its behaviour as it opens.

2.1 Mobility

In order for a mechanism to function, it must have a mobility of at least, and ideally no more than 1. The mobility is given by the Maxwell count for the mechanism. That is the number of degrees of freedom minus the number of constraints. A mobility of 0 means that a mechanism is rigid and therefore not actually a mechanism, a mobility of 1 gives a mechanism that has one possibly movement, such as a trellis structure. The mobility is equal to the number of internal degrees of freedom, i.e. the degrees of freedom excluding rigid body rotation and translation.

For a general ring of n bars, before they are connected each bar in the ring has 6 degrees of freedom (3 rotational, 3 translational). Connecting each hinge removes 5 degrees of freedom from the system, and fixing one of the bars in space to prevent rigid transformation of the entire mechanism removes a further 6 degrees of freedom. So to give one remaining degree of freedom after the ring is connected - the deployment mechanism - n must satisfy

$$6n - 5n - 6 = 1 \quad \Rightarrow \quad n = 7 \tag{2.1}$$

Clearly the four-bar mechanism has less than seven bars yet still has an internal mechanism. This is possible because of its planes of symmetry. There is actually only one

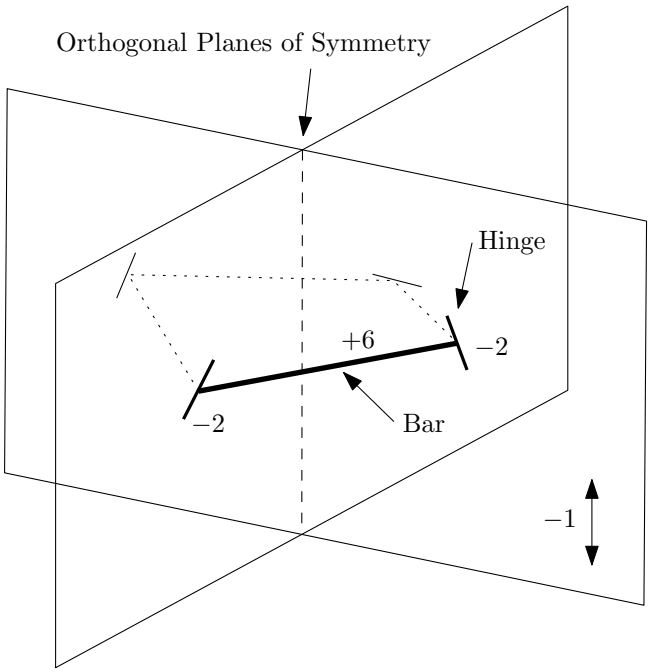

Figure 2.1: Square four-bar mechanism mobility. The solid bar has 6 degrees of freedom unconstrained. Constraining its end hinges to lie in the symmetry planes removes four degrees of freedom (two for each hinge). Constraining the entire mechanism's vertical position removes another degree of freedom leaving the mechanism with a mobility of 1. The dotted bars are merely mirror images of the solid one and are not independent of it.

independent bar - the others are mirror images of it. The independent bar starts with 6 degrees of freedom. For each of the hinges that must be constrained to a plane (the planes of symmetry), 2 degrees of freedom are removed. A further degree of freedom is removed by fixing the height of the mechanism, leaving 1 degree of freedom for the deployment mechanism (see figure 2.1).

For a mechanism with equal length bars to give a 2:1 rectangle at least six bars must be used, so it must have at least one plane of symmetry. To give a 3:1 rectangle at least eight bars must be used. This means a 3:1 rectangle must have a mobility of at least 2 and would require extra constraint elements to reduce its mobility to 1. I will later be shown that a mechanism with six bars and one plane of symmetry has a mobility of 1.

2.2 Geometry

The geometry of the family of mechanisms is shown in figure 2.2. The mechanisms behaviour is altered by varying the geometry parameter α between 0 and $\frac{\pi}{2}$. This parameter alters the angle of all the bars in the frame, and hence the orientation of the hinges. The angles made by the hinges, measured in a plane orthogonal to their axis are ψ_a and ψ_b (see figure 2.3). Thus, $\psi_a = \psi_b = 0$ when the mechanism is closed. Opposite hinges always

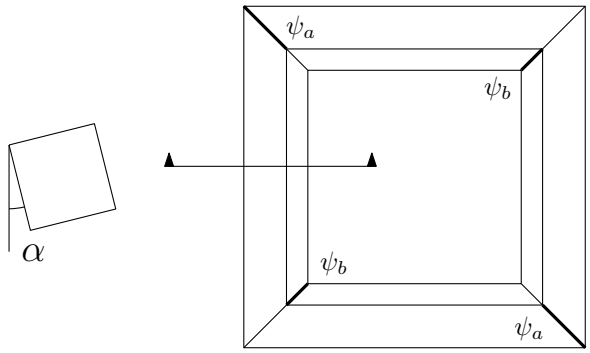

Figure 2.2: Geometry of the square four-bar mechanism in an open configuration. ψ_a and ψ_b define the hinge angles and are 0 when the mechanism is closed. α affects the geometry of the mechanism allowing a family of similar frames to be defined.

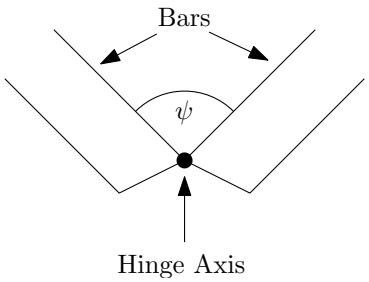

Figure 2.3: The hinge angles are measured as the angle between the bars, looking along the hinge axis.

have the same value due to the symmetry of the mechanism.

Changing α affects how the mechanism opens and how the hinge angles ψ_a and ψ_b depend on one another. The relationship between ψ_a and ψ_b was calculated for different α values and is shown in figure 2.4. It can be seen from the graph that altering α changes the maximum values of ψ_a and ψ_b, and also the degree of coupling between them. For example, with α close to zero ψ_b increases rapidly to $\frac{\pi}{2}$ with little change in ψ_a. When $\alpha = \frac{\pi}{4}$ a change in one angle causes a similar change in the other.

The relationship between ψ_a and ψ_b was calculated by representing the hinge vectors and rotations as quaternions. Quaternions are an extension of complex numbers that allow easy representation of rotations algebraically (see Appendix A and [7]). The Maxima[1] computer algebra system was then used with the code in Appendix B to find an explicit formula relating ψ_a to ψ_b.

A rectangular mechanism cannot be made with four bars and still fit together in a folded state. It requires at least six bars where the long sides consist of two bars. As well as a square mechanism, hexagonal and octagonal versions mechanisms are possible, but there is no obvious way to extend any of these mechanisms to form a rectangle. An alternative square mechanism that can be extended to form a rectangle in a more obvious fashion will now be discussed.

[1]Available from `http://maxima.sourceforge.net/`.

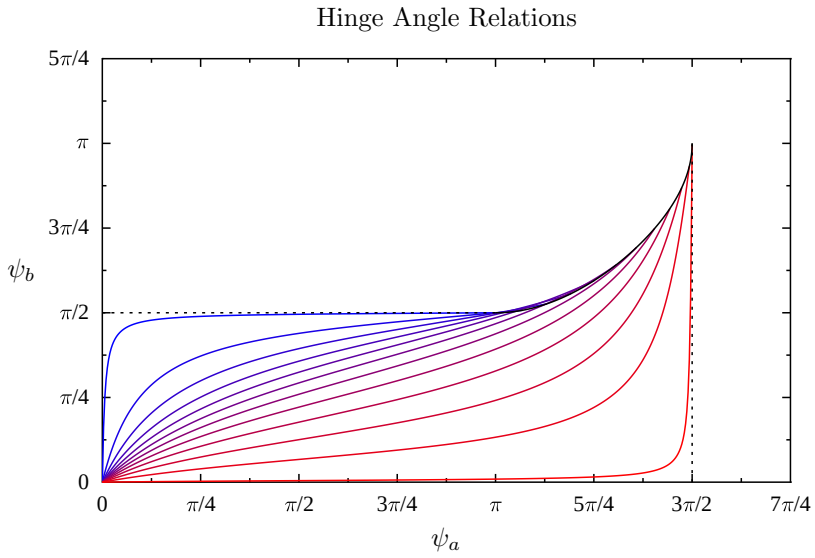

Figure 2.4: Relationship between hinge angles as the four-bar mechanism opens. Each line is for a different value of α from 0 (blue) to $\frac{\pi}{2}$ (red) in equal steps. The mechanism is closed when the hinge angles $\psi_a = \psi_b = 0$.

Chapter 3

The Square Six-Bar Mechanism

A square six-bar mechanism was invented by Guest in 1999 [5]. It consists of two long bars and four short ones of half the length. The mechanism is shown in figure 3.1.

There are now two geometry parameters α and β that can be altered to give different variations of the frame. In order to investigate the effects of changing α and β it was first necessary to calculate the position of the plane of symmetry A-A in terms of α, β, and the hinge angles ψ_a and ψ_b (see figure 3.2).

The method used to generate the geometry of the mechanism with basic geometric operations follows. This is required to find the hinge angles, and to render pictures of the mechanism.

3.1 Geometry

For this it shall be assumed that the mechanism stays symmetric, although later it will be shown that this is not always true. The geometry of the mechanism can be generated numerically by rotating and projecting various points. The following method was used to construct the mechanism and find the position of the plane of symmetry. It is assumed that one of the end bars is fixed, so the plane of symmetry moves as the mechanism opens.

Start with a square in the X-Z plane. Rotate it by α. Next project it onto two 45° planes as shown in figure 3.3 a and b. This completes one long bar. To make the two short bars reflect half of the long bar about its top face, and then twist the bar by $\alpha - \beta$ as shown in figure 3.3 c and d. This gives one half of the closed mechanism. The mechanism can be opened by rotating both short bars about their hinges by the desired angle of opening, ψ_a. The symmetry plane can now be easily found by using the cross product of the directions of the hinges. The bars can then be reflected in the symmetry plane to give the complete mechanism and the value of ψ_b.

ψ_b varies from 0 to π as the mechanism opens in all cases, but what about the other hinges? The maximum angle of ψ_a in terms of α was calculated as follows.

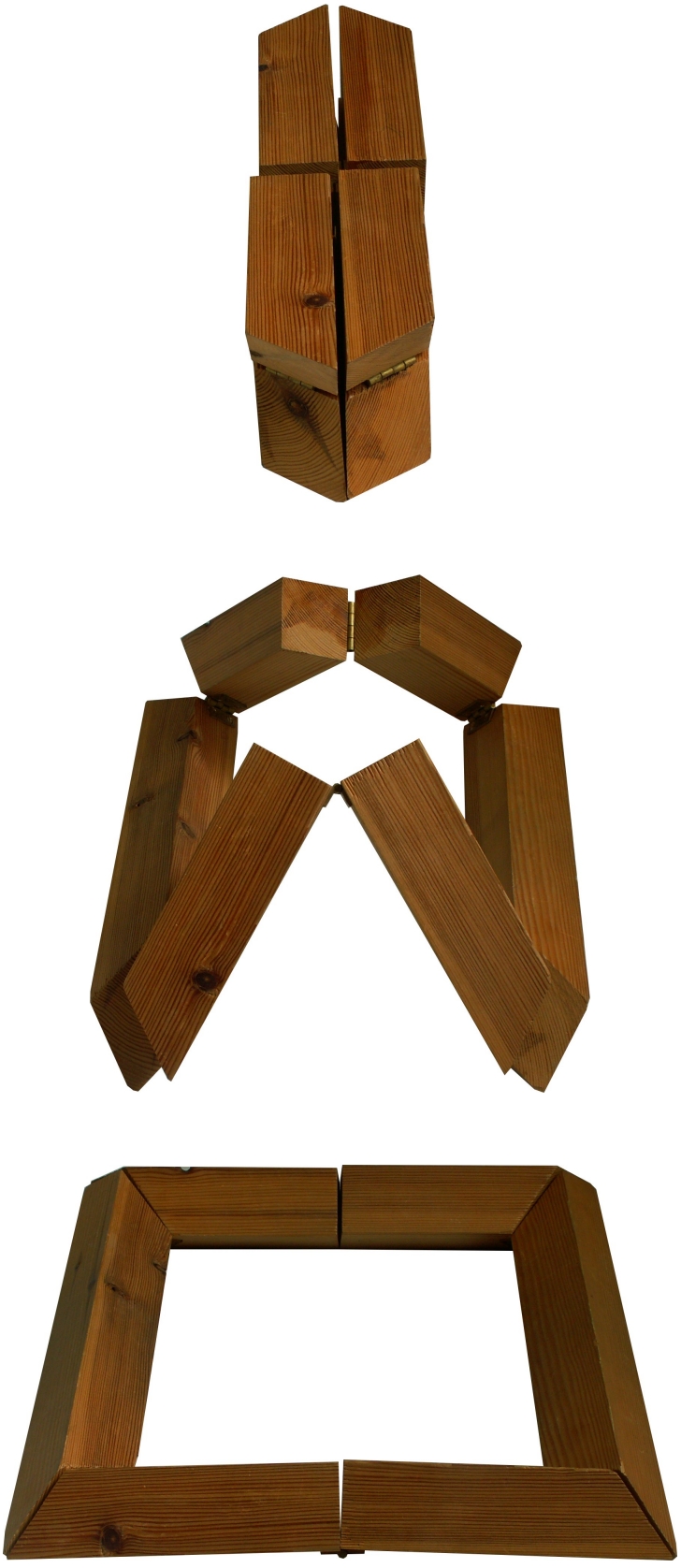

Figure 3.1: Guest's square six-bar mechanism.

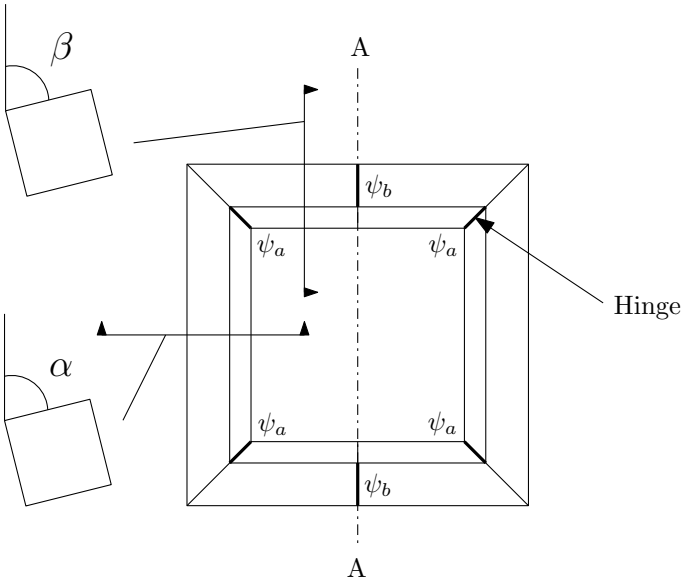

Figure 3.2: Geometry of the square six-bar mechanism. There are now two geometry parameters α and β. These can be changed independently (causing a twist in the short bars). ψ_a and ψ_b define the hinge angles and are 0 when the mechanism is closed as before.

First take the cross section A-A through the frame as shown in figure 3.4 a) and c). This gives a square rotated by α. Taking a cross section through the hinge at 45° has the effect of stretching the square horizontally by $\sqrt{2}$. Thus the angle of the hinge to the vertical is

$$\xi = \tan^{-1}\left(\frac{\tan\alpha}{\sqrt{2}}\right) \tag{3.1}$$

Next, define the length of the hinge as a. Its length projected onto the edge of the bar is $\frac{a\cos\gamma}{\sqrt{2}}$ as shown in figure 3.5 a). This allows us to form a right angled triangle on the surface of the bar and find θ.

$$\theta = \cos^{-1}\left(\frac{\cos\xi}{\sqrt{2}}\right) \tag{3.2}$$

Finally a triangle can be formed with sides $\sin\theta$, $\sin\theta$ and $\sqrt{2}$ that is orthogonal to the hinge, and gives the value of ψ_a in the mechanism's deployed state (figure 3.5 d).

$$\psi_{\max} = \sin^{-1}\left(\frac{1}{\sqrt{2}\sin\theta}\right) \tag{3.3}$$

Substituting in values, and using some mysterious trigonometric identities gives

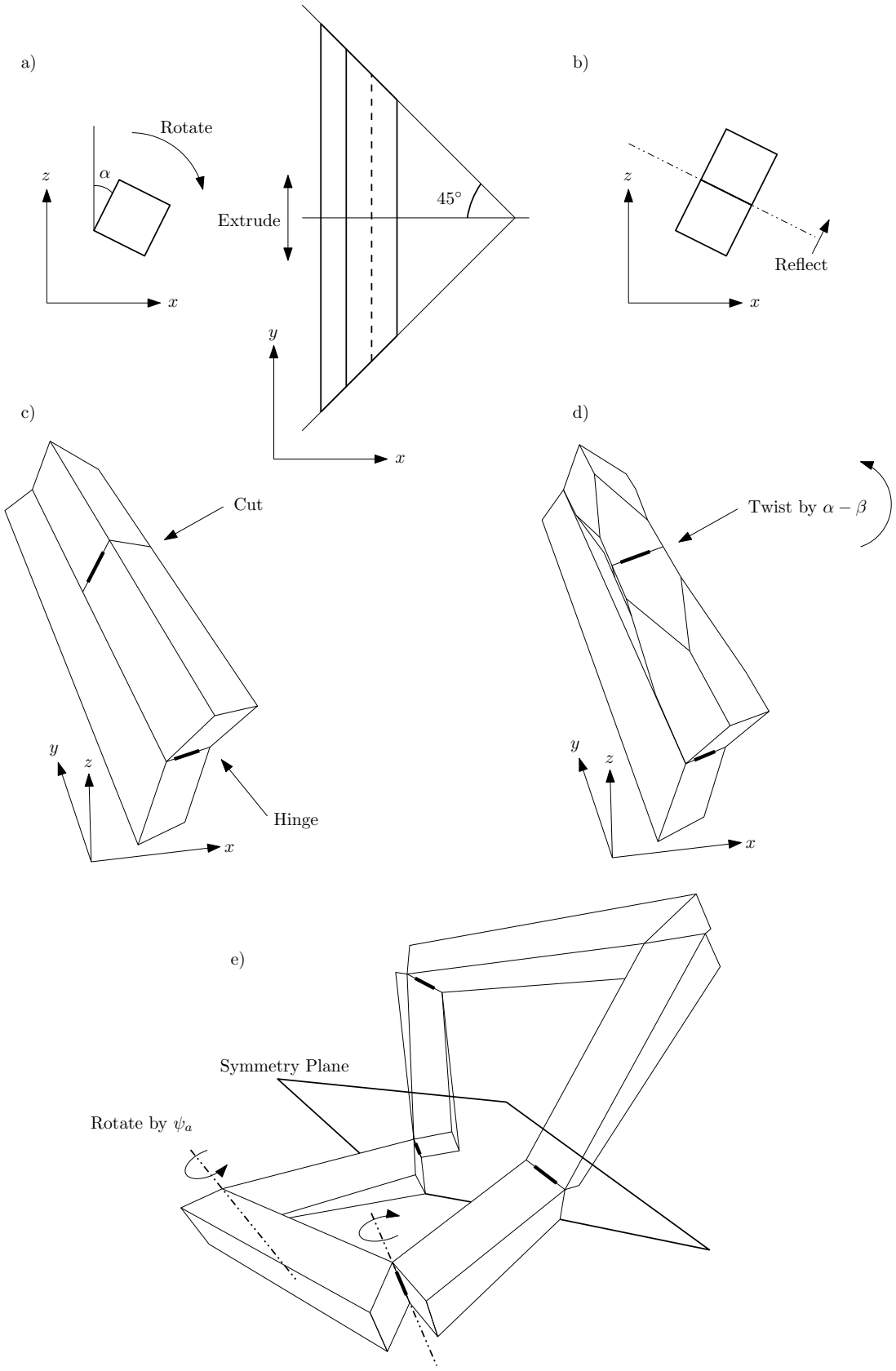

Figure 3.3: Generation of the square six-bar mechanism geometry. One half is generated geometrically and used to find the position of the plane of symmetry. The half-mechanism is then reflected to give the complete structure.

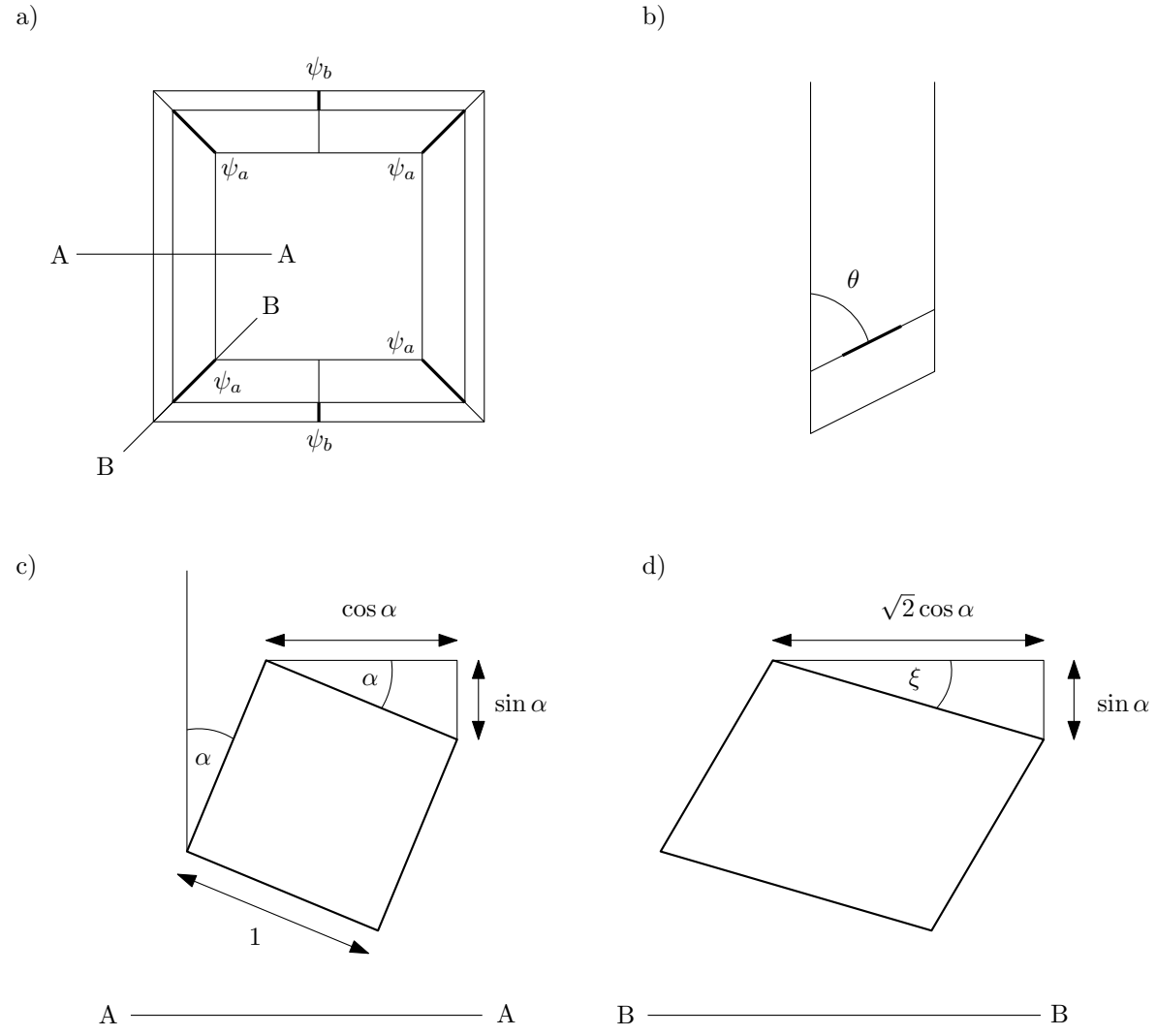

Figure 3.4: Calculation of the maximum hinge angles.

$$\psi_{\max} = 2\sin^{-1}\left(\sqrt{2}\sin\cos^{-1}\left(\frac{\cos\tan^{-1}\left(\frac{\tan\alpha}{\sqrt{2}}\right)}{\sqrt{2}}\right)\right)^{-1} \tag{3.4}$$

$$= \pi - \cos^{-1}(\cos^2\alpha) \tag{3.5}$$

This value is correct for $0 \leq \alpha \leq \pi$. For $-\pi \leq \alpha \leq 0$ the result is $\psi_{\max} = \pi + \cos^{-1}(\cos^2\alpha)$.

The position of the symmetry plane was also found using quaternions (see Appendix B) to give an explicit formula for ψ_b in terms of ψ_a, α and β for the slightly simpler case $\alpha = \beta$. This formula was used with Pov-Ray[1] to render videos of the mechanism unfolding for different values of $\alpha = \beta$. Some frames from the animations are shown in figure 3.6. This also served as a useful check of the results. Only 5 of the hinges are used - the fact

[1]A ray tracing program available from `http://www.povray.org/`.

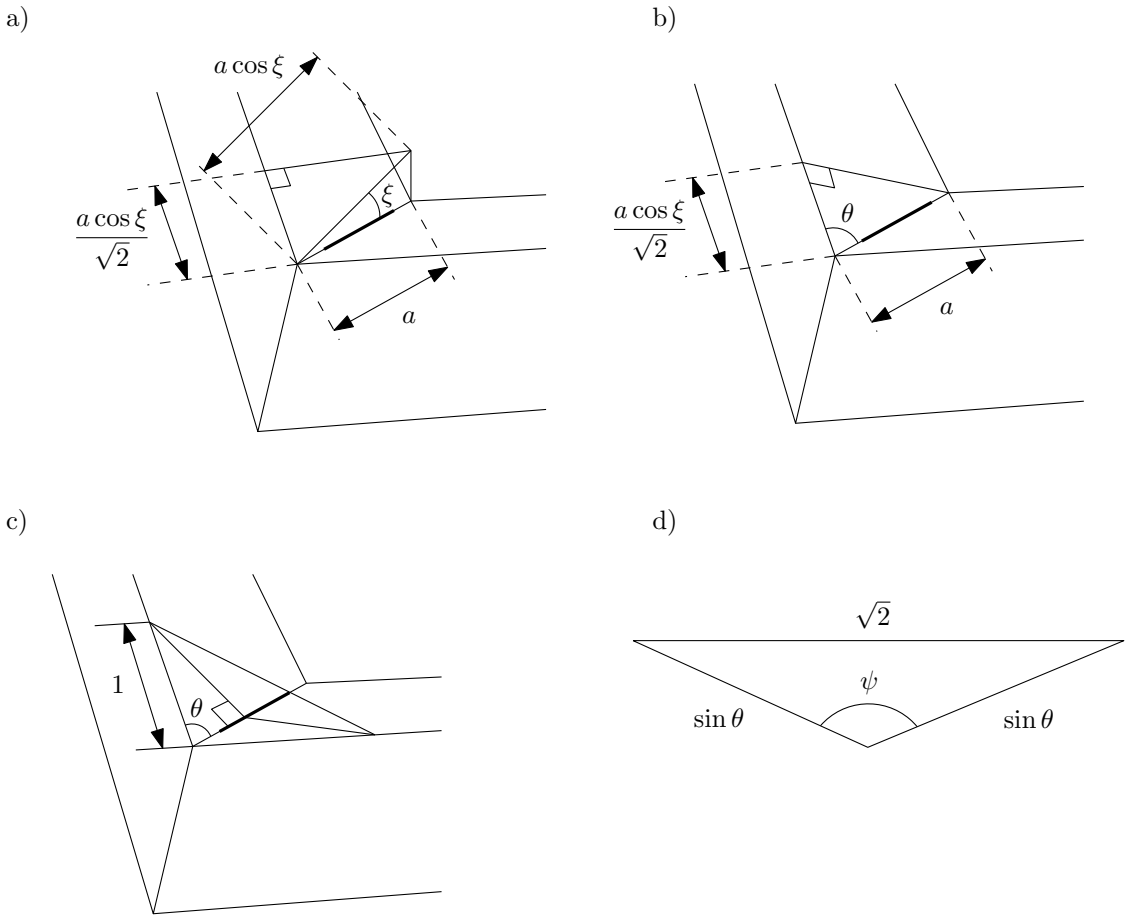

Figure 3.5: Calculation of the maximum hinge angles (continued).

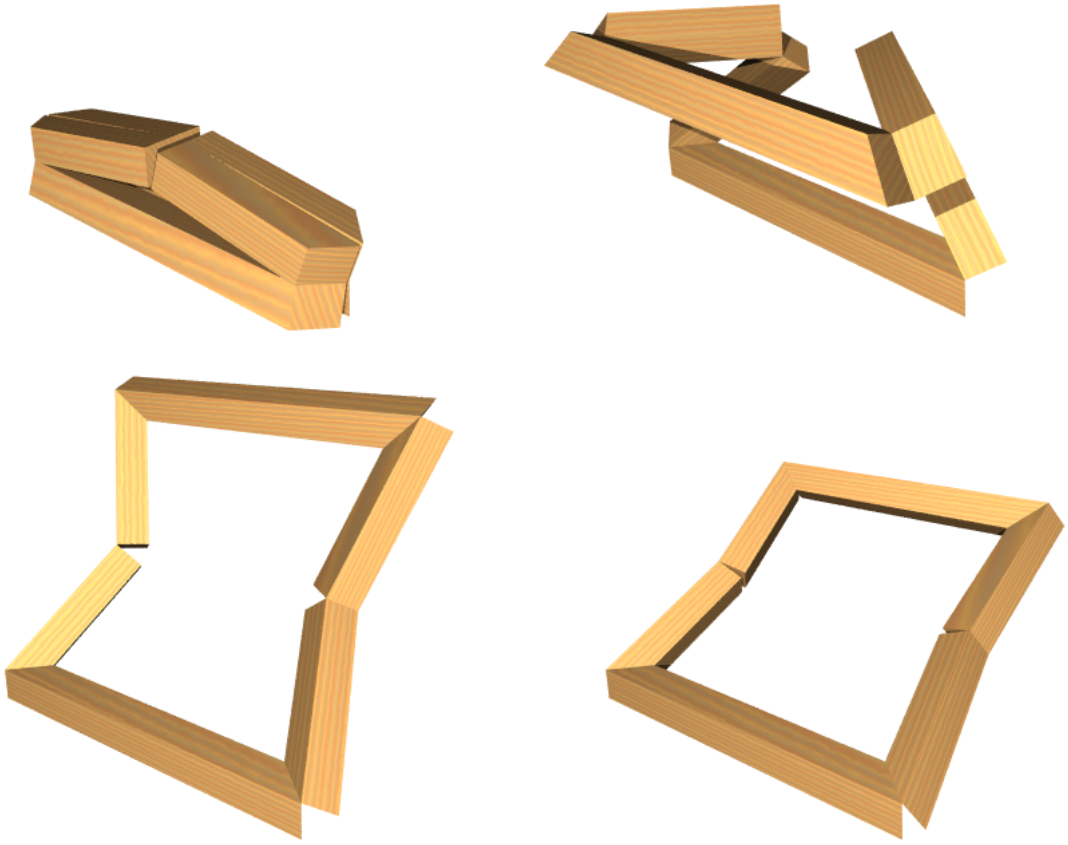

Figure 3.6: Computer renders of the square six-bar mechanism produced using Pov-Ray.

that the sixth lines up indicates that the calculated hinge angles are correct.

Raytracing is a slow process, so an interactive 3D computer program was written that allows the user to change α, β, and ψ_a and immediately see the result[2]. A screenshot is shown in figure 3.7.

This program proved to be very useful. After experimenting with various values of α and β the following results were found:

1. Values of $\alpha < 0$, $\beta < -\pi$ or $\beta > \pi$ give a mechanism that passes through itself.
2. Values of $\beta > \alpha$ give a mechanism that passes through itself.
3. At $\beta = -\pi$ and $\beta = \pi$ the two middle hinges can become collinear and the mechanism misbehaves.
4. At $\alpha = 0$ and $\alpha = \pi$ the corner hinges become collinear giving a second unwanted mechanism.

[2]All the programs written are available from `http://www2.eng.cam.ac.uk/~tdh29/`.

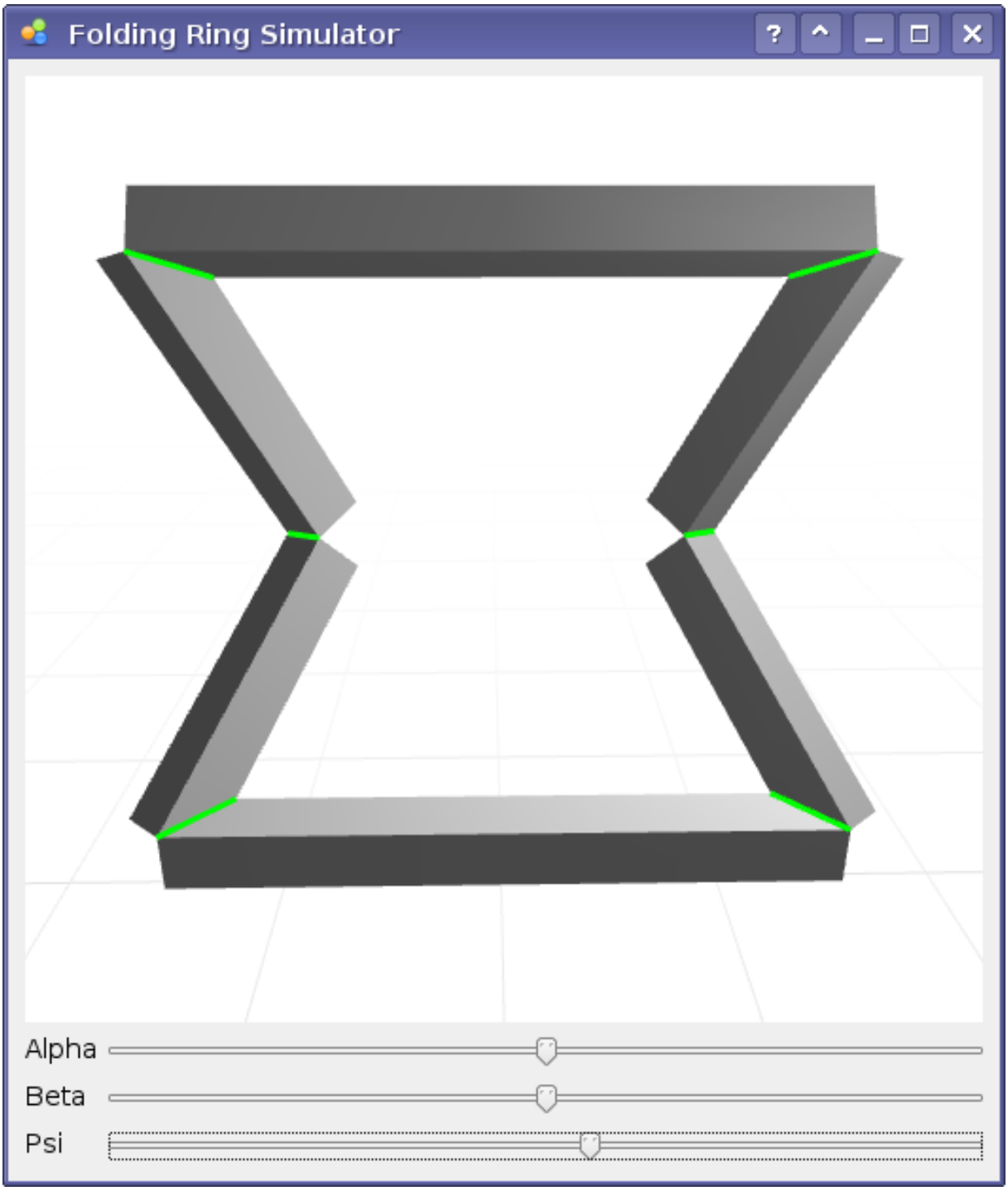

Figure 3.7: Real-time 3D simulation of the six-bar mechanism. The view can be rotated and zoomed, and the parameters altered using the sliders at the bottom. The hinges are shown as green lines.

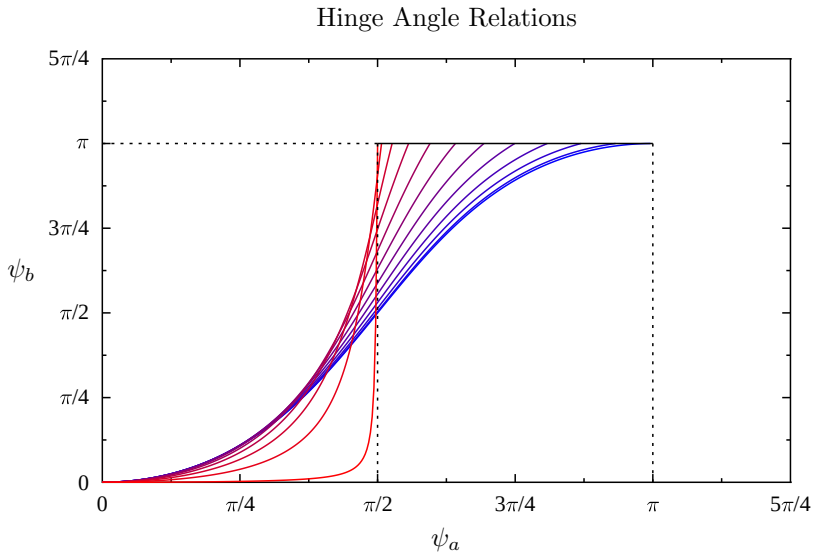

Figure 3.8: Hinge angle relationships for Guest's mechanism for the case $\alpha = \beta$. Each line shows a mechanism with a different value of $\alpha = \beta$ from 0 (blue) to $\frac{\pi}{2}$ (red) in equal steps. The mechanism is closed at $\psi_a = \psi_b = 0$ and deployed at the line $\psi_b = \pi$, $\frac{\pi}{2} \leq \psi_a \leq \pi$.

Combining the above gives the result that working mechanisms must have: $0 < \alpha < \pi$, $-\pi < \beta < \pi$ and $\beta \leq \alpha$. This is a sufficient as well as necessary condition.

The formula mentioned previously was used to produce a graph of the relationship between ψ_b andψ_a for various values of $\alpha = \beta$ (figure 3.8).

Chapter 4

The Rectangular Mechanism

To extend the six-bar square mechanism to form a rectangle it was envisaged that the short bars could be extended to the same length as the long ones. This would indeed give a working mechanism that formed a 2:1 rectangle if the bars were allowed to pass through each other. To fix this problem, different values of α and β must be used for each end of the mechanism as shown in figure 4.1.

By considering the closed state of the mechanism, it is clear that for the central hinges to lie in a plane, β_1 and β_2 cannot be independent. To account for this, a new parameter γ was defined such that:

$$\begin{aligned} \beta_1 &= 2\alpha_1 - \gamma \\ \beta_2 &= 2\alpha_2 - \gamma \end{aligned} \tag{4.1}$$

This ensures that the hinges are always coplanar when the mechanism is closed. They are coplanar when the mechanism is open by definition.

Mechanisms of this type have previously been made with flexible members, but so far no geometry has been found that allows stress-free deployment [11]. It will now be confirmed that a mechanism of this type has a mobility of 1, a necessary condition for successful deployment.

4.1 Mobility

The Maxwell count can be used to show that the mechanism has a mobility of 1 and is truly a mechanism. A rectangular six-bar mechanism has only one plane of symmetry, so there are 3 independent bars. Each has 6 degrees of freedom, -5 each for the two intermediate hinges, -2 each for the two hinges on the symmetry plane, and -3 to fix the position and orientation of the mechanism on the symmetry plane leaves 1 internal degree of freedom. This is shown in figure 4.2. A more rigorous analysis of the mobility of symmetric mechanisms is given in [3].

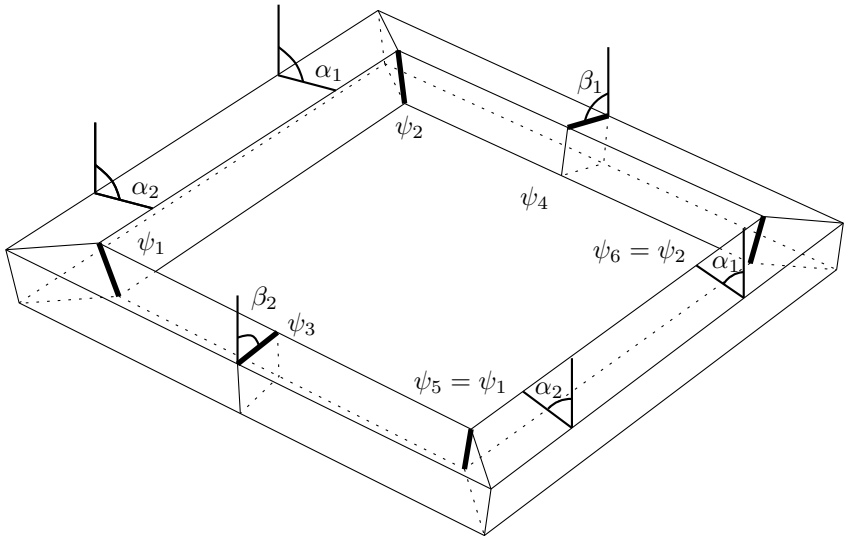

Figure 4.1: Geometry of the rectangular six-bar mechanism. There are now four geometry parameters - α_1, α_2, β_1, and β_2. Differences in the values create twists in the bars (not shown). There are nor four different hinge angles are: ψ_1, ψ_2, ψ_3, and ψ_4.

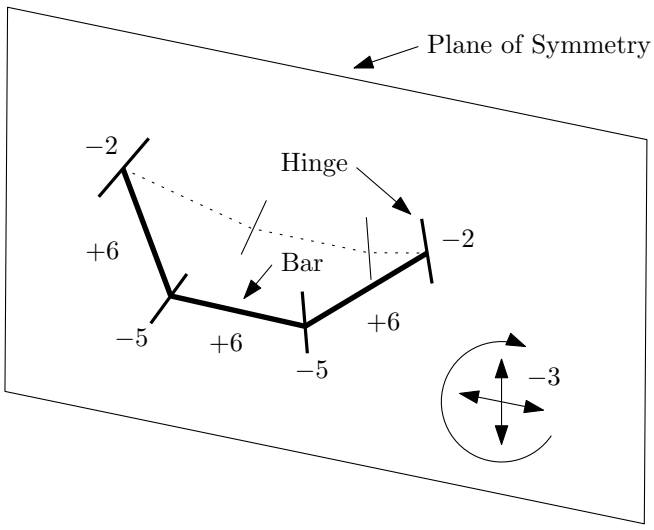

Figure 4.2: Rectangular six-bar mechanism mobility. In this case there is only one plane of symmetry and three independent bars. Each bar starts with 6 degrees of freedom and 14 are removed by constraining the hinges. 3 further degrees of freedom are removed by fixing the mechanism's position and orientation on the plane of symmetry, leaving a mobility of 1.

A mobility of 1 is a necessary but not sufficient for a mechanism to work. There must also be a continuous path from open to closed states without self-intersection. In order to find the mechanisms for which this is possible it is necessary to calculate the position of the plane of symmetry.

4.2 Symmetry Plane Calculation

In order for the mechanism to work, it must be possible to choose compatible values of ψ_1 and ψ_2 such that the central hinges remain coplanar as the mechanism opens. The plane they lie in is the plane of symmetry. Finding ψ_1 as a function of ψ_2 is not a trivial problem. The hinges will be in a plane when their axes (extended to infinity) intersect. The problem is equivalent to the following: Three arbitrary lines are positioned in 3D space. One is fixed and another is a fixed axis of rotation. The problem is the find the angle such that the third line can be rotated around the second to intersect the first. The shape swept by rotating a straight line in space is a hyperboloid, and the problem simplifies to finding the intersection of two arbitrary hyperbola with the same axis. In general there are two cases: either there are no angles that cause them to intersect, or they intersect twice giving two angles. These angles are sometimes the same as in $x^2 = 0$.

By expressing this problem using quaternions, and using the Maxima computer algebra package it was possible to find an extremely long but explicit formula for these two angles. This is useful as it is much faster and more reliable than using iteration, and thus allows real-time simulation. Once the angles have been found the plane of symmetry can easily be calculated in each case in the same way as the square six-bar mechanism. It also allows calculation of the mechanism paths - that is the path the values of ψ_1 and ψ_2 follow as the mechanism unfolds.

4.3 Mechanism Paths

As the mechanism unfolds, for each angle ψ_2 there are either zero, one or two possible angles for ψ_1 that result in a compatible geometry. The same is true for ψ_1 in terms of ψ_2. These compatible values can be plotted to give mechanism paths. ψ_3 and ψ_4 also change as the mechanism opens but these are not considered in the following analysis. There are several distinct cases that can occur. For simplicity the fact that many configurations are impossible due to the structure intersecting itself will be ignored.

4.3.1 A Single Mechanism Path

In some cases there is a single cyclic mechanism path. An example is shown in figure 4.3. It must go through the closed and deployed configurations. If it goes from one to the

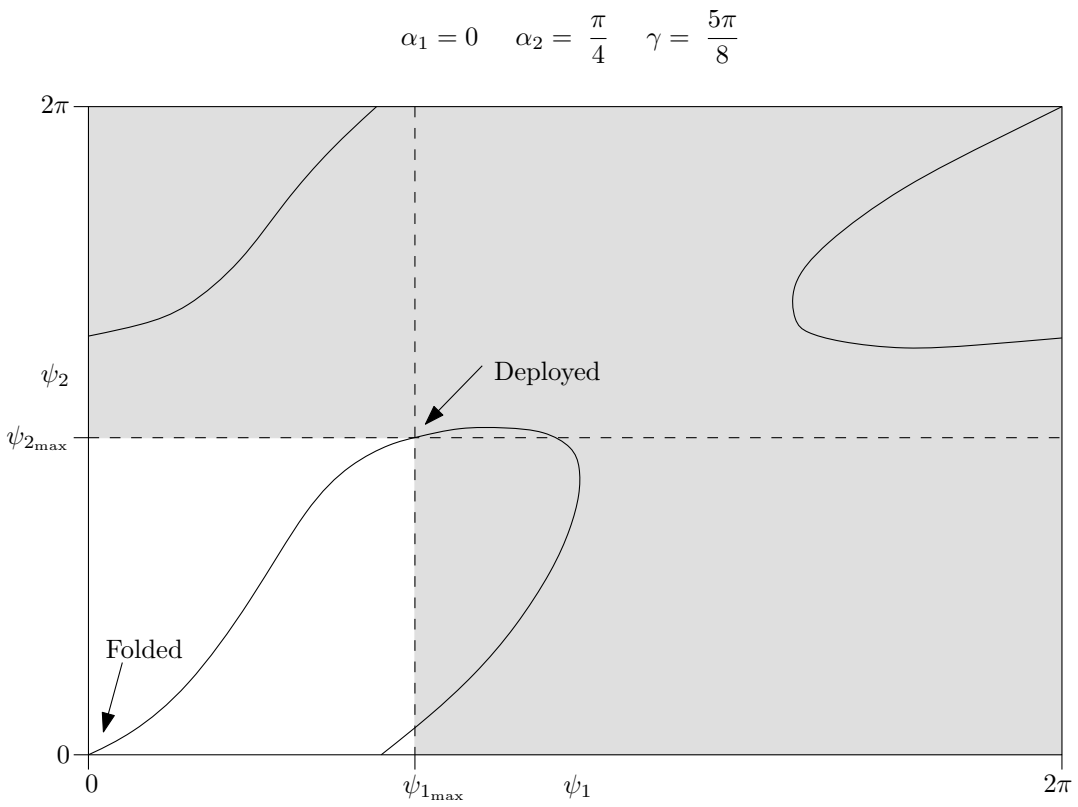

Figure 4.3: A single mechanism path. The grey area denotes the region for which ψ_a or ψ_b are above their maximum values and hence cannot be reached. The mechanism is closed when $\psi_1 = \psi_2 = 0$ and follows the path shown until it is open at $\psi_1 = \psi_{1_{\max}}$, $\psi_2 = \psi_{2_{\max}}$.

other with allowable hinge angles (the white area in the figures) then the mechanism is likely to work.

4.3.2 An Intersecting Mechanism Path

In other cases there is a single self-intersecting mechanism path (figure 4.4). All of the mechanisms with $\alpha_1 = \alpha_2$ (and hence the square six-bar mechanisms) fall into this category, although sometimes the bifurcations occur at unreachable hinge angles. For mechanisms with $\alpha_1 = \alpha_2$ there is a certain point at which an asymmetric mechanism crosses the symmetric one. This is undesirable as potentially the wrong path could be followed during deployment. If the bifurcation occurs far outside the reachable hinge angles then it is unlikely to be a problem. These results were also found by Gan and Pellegrino [4].

4.3.3 Two Separate Mechanism Paths

Finally, there can be two separate mechanisms (figure 4.5). Most of the useful mechanisms fall into this category with one mechanism going from start to finish. However if deployed state is on one mechanism path, and the closed state is on the other path then the

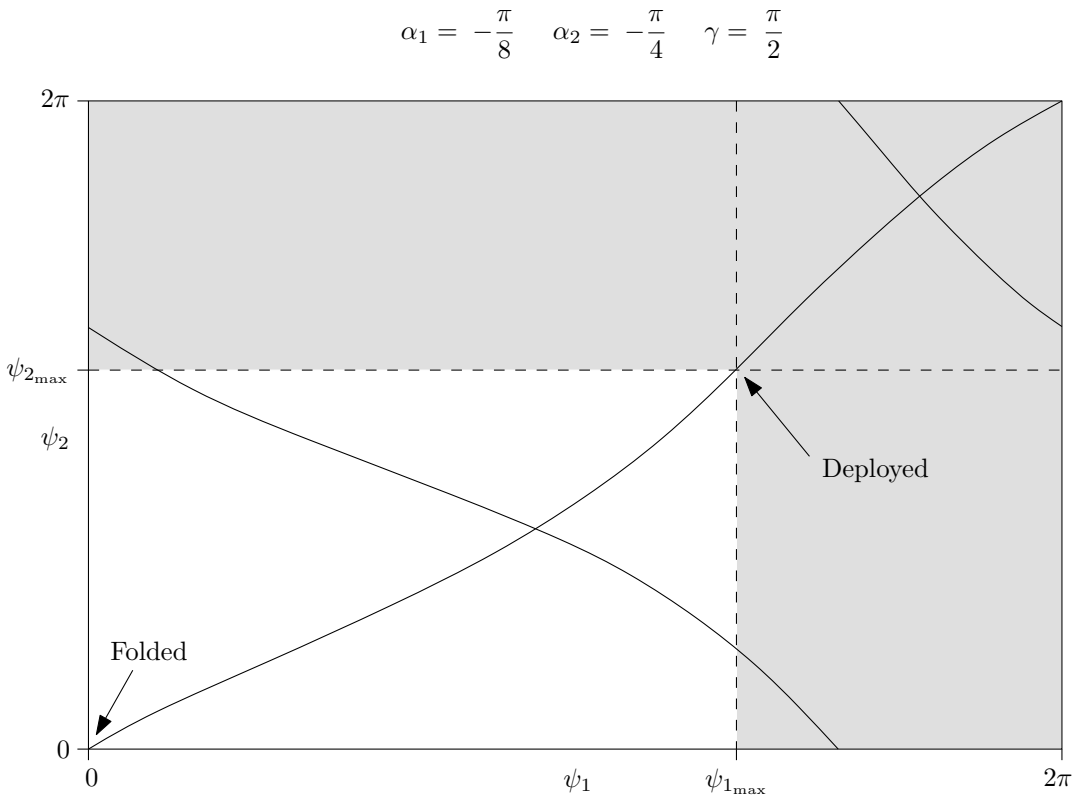

Figure 4.4: A single self-intersecting mechanism path. At the point of intersection there are four possible directions that the mechanism can move, rather than the usual two. If the mechanisms intersect then there are always two points of intersection.

mechanism will not work as there is no way to jump between them. An example of this is shown in figure 4.6.

These graphs are equivalent to the graphs of figure 2.4 and 3.8 for the square mechanisms. They provide an additional check of whether a mechanism will work that will be used later to find values of α, β and γ that give working mechanisms. Singular value decompositions will now be used to look at the bifurcation of the mechanism paths in more detail.

4.4 Singular Value Decomposition

In order to prevent failure during unfolding there must be only one set of compatible small changes in hinge angles that are as the mechanism unfolds. If at any point the bars have more than one possible motion then they may travel along the wrong mechanism path and end in a wrong configuration. To test how likely this is, the Singular Value Decomposition (SVD) of a matrix relating hinge rotations to distortion of the bars must be calculated.

For a given configuration, the mechanism can be cut at an arbitrary point and one end of the resulting chain fixed. The effect on the free end of changing the hinge angles

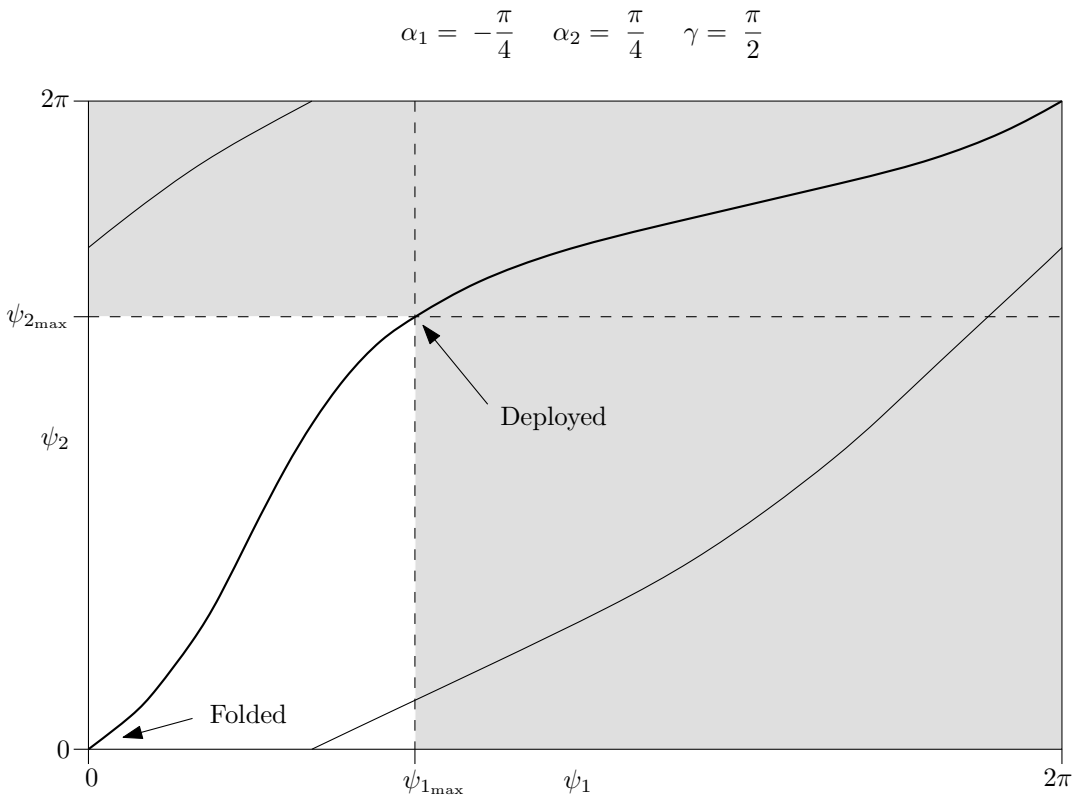

Figure 4.5: Two separate mechanism paths. It is impossible to reach one mechanism from the other without dismantling the mechanism and rebuilding it in a different configuration, even if you allow the hinges to open past their physical limits.

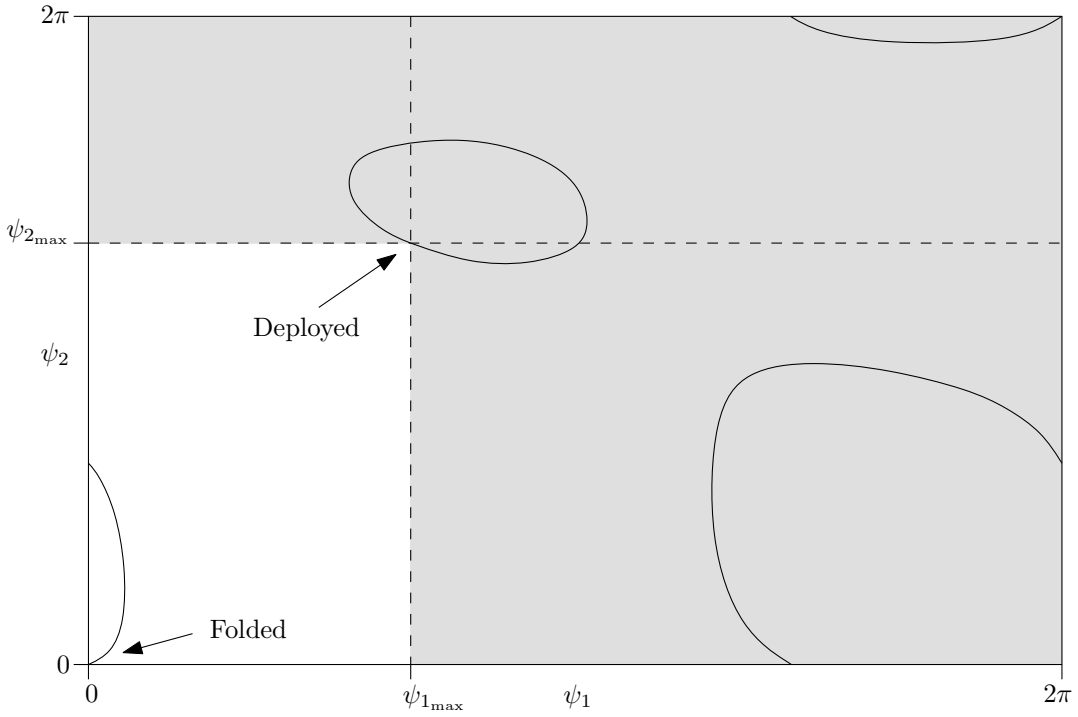

Figure 4.6: Two separate mechanism paths. In this example there isn't a single mechanism that goes from the folded to deployed states so the mechanism cannot open (or close if it starts open).

by small amounts can be calculated and expressed in matrix form:

$$[M] \times \delta \begin{bmatrix} \psi_1 \\ \psi_2 \\ \psi_3 \\ \psi_4 \\ \psi_5 \\ \psi_6 \end{bmatrix} = \delta \begin{bmatrix} x \\ y \\ z \\ \theta_x \\ \theta_y \\ \theta_z \end{bmatrix} \tag{4.2}$$

Where for hinges with positions $\mathbf{r_n}$ and directions $\mathbf{h_n}$, $[M]$ is given below. Note that the rotations are small so they can simply be summed.

$$[M] = \begin{bmatrix} | & | & | & | & | & | \\ \mathbf{r_1} \times \mathbf{h_1} & \mathbf{r_2} \times \mathbf{h_2} & \mathbf{r_3} \times \mathbf{h_3} & \mathbf{r_4} \times \mathbf{h_4} & \mathbf{r_5} \times \mathbf{h_5} & \mathbf{r_6} \times \mathbf{h_6} \\ | & | & | & | & | & | \\ | & | & | & | & | & | \\ \mathbf{h_1} & \mathbf{h_2} & \mathbf{h_3} & \mathbf{h_4} & \mathbf{h_5} & \mathbf{h_6} \\ | & | & | & | & | & | \end{bmatrix} \tag{4.3}$$

Any movement will require the small changes in hinge angle to be in the null space of $[M]$, giving zero movement for the free end of the chain. If $[M]$ has a rank of 6, then there are no possible values and the mechanism cannot move. If it has a rank of 5 then there is one mechanism, and if it is less than 5 then there are more. Thus it is desirable that the rank is as close to 5 as possible.

The rank of the matrix can be measured by taking its SVD. As $[M]$ never has a rank of 6, the sixth SVD value will always be zero. The fifth value gives the degree that there is another undesirable mechanism. Ideally it should be as high as possible. If it ever reaches zero then there are two mechanisms for this point and the mechanism could deploy incorrectly.

The fifth SVD value has been plotted along with the mechanism paths for two frames in figure 4.7. It can be seen that there is a dip in the value when the two mechanisms are close. At this point it would be possible to jump from one mechanism to the other by bending the frame a little.

4.5 Geometry

To find values of α_1, α_2 and γ that give a working mechanism the simulation program mentioned previously was updated to use the new rectangular geometry. The first working values were found by snapping their values to 45° increments and trial and error. A wooden model of the first mechanism found is shown in figure 4.8. Several others were also found by this method (see table 4.1) but there was no clear pattern as to which values

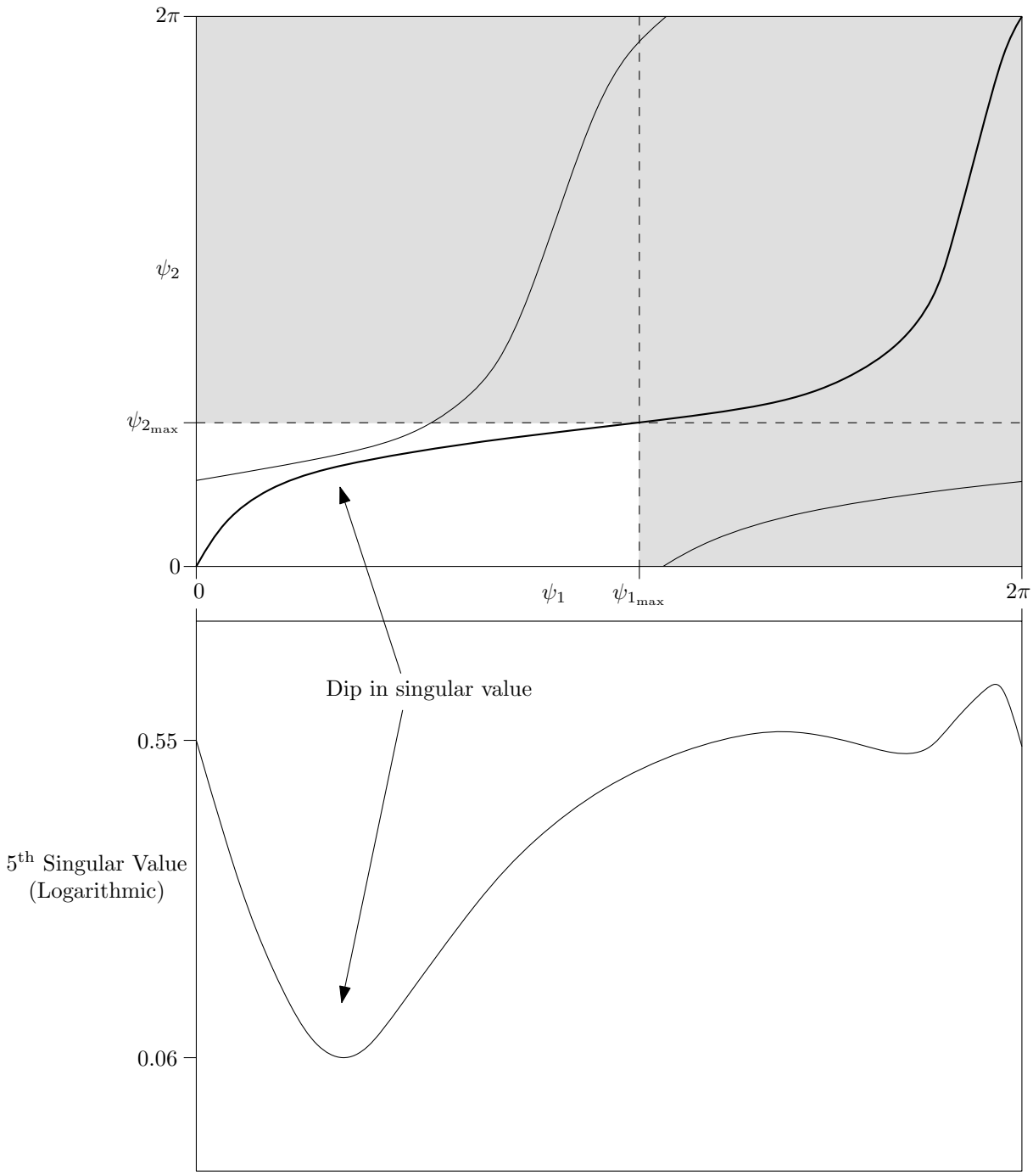

Figure 4.7: Fifth singular value as the mechanism unfolds. The dip in value corresponds with the proximity of the two mechanisms. At this point it would be possible to jump between the mechanisms by bending the bars slightly. The singular value becomes zero if the mechanism paths ever intersect.

α_1	α_2	γ
0.25π	-0.25π	0.5π
0	-0.25π	0.5π
0.5π	-0.25π	0.5π
0.25π	-0.5π	0.375π
0.25π	-0.25π	0.375π

Table 4.1: Some initial rectangular mechanisms.

work.

To try and find the other working mechanisms, or at least narrow down the possibilities, a program was written to check for each set of geometry values whether it resulted in a isolated complete mechanism as described above[1]. The results are shown in figure 4.9. A detailed view of a single slice through the α_1, α_2, γ parameter space is shown in figure 4.10. The program also calculates the minimum value of the fifth singular value as the mechanism unfolds. This is shown as the grey level of the image, with black representing zero. The pattern is still not clear but there are some things that can be noted.

1. The images are symmetric about $\alpha_1 = \alpha_2$ as expected[2]. Swapping their values just creates a mirror of the mechanism.

2. There are two main regions of the space. The square central area, and the side shapes. Guest's square six-bar mechanism lies in the square region (as $\alpha_1 = \alpha_2$). The mechanisms in this region have α_1 similar to α_2. This means that the mechanism arms clash and cannot close.

3. All the working mechanism have $-\frac{\pi}{2} \leq \alpha_{1,2} \leq \frac{\pi}{2}$.

The shape depicted represents a superset of the actual working mechanism values because some of the values give self-intersecting mechanisms. This information was used to find the mechanism with the highest minimum SVD as it unfolds (the whitest point figure 4.9). This mechanism is shown in figure 4.11.

This is only one possible optimisation. It may be that other parameters are important, such as the maximum degree of stretching a membrane would undergo if attached to the frame. Another possible optimisation parameter is the minimum degree of coupling between the hinges as they open, for example

$$\min \left(\frac{\dot{\psi}_i}{\dot{\psi}_j} \right) \qquad i, j \in 1, 2, 3, 4 \qquad i \neq j \tag{4.4}$$

Another interesting property is that only some of the frames keep the end bars parallel as they open. The mechanism shown in figure 4.12 has very non-parallel end bars.

[1]Note that the program only checks that the maximum angles of ψ_1 and ψ_2 are not exceeded. It would

Figure 4.8: The first successful rectangular frame.

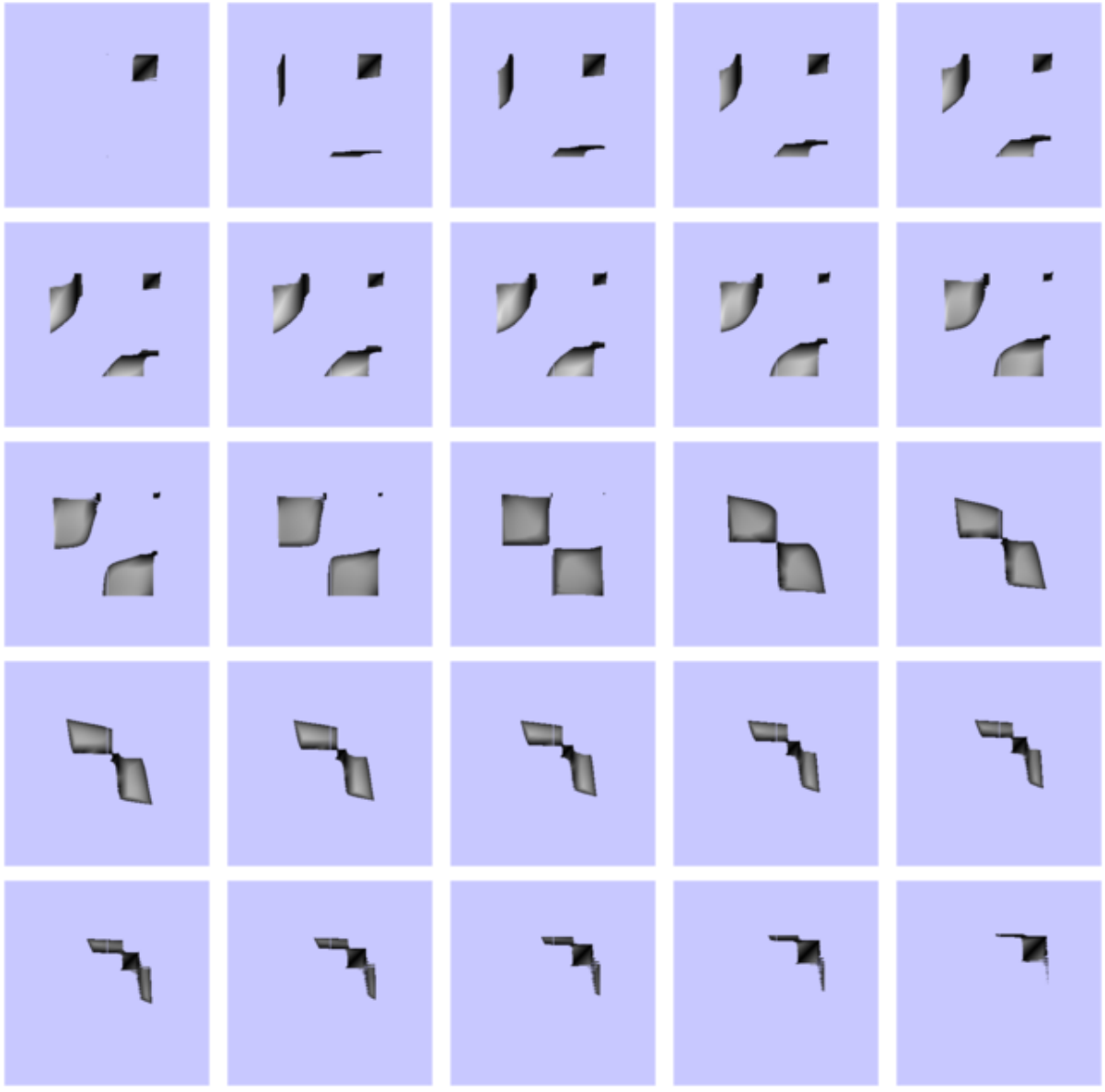

Figure 4.9: A superset of the useable geometry values. γ is constant within each image and varies from 0 in the top left image to π in the bottom right. Within each image, α_1 goes from $-\pi$ to π on the x axis, and α_2 goes from $-\pi$ to π on the y axis. Blue areas indicate mechanisms without a complete non-intersecting path from closed to open. The grey level indicates the minimum level of the 5th singular value during opening, with black representing zero. The set repeats for $-\pi \leq \gamma \leq 0$. A more detailed view of the slice for $\gamma = 0.5\pi$ (the central image) is shown in figure 4.10.

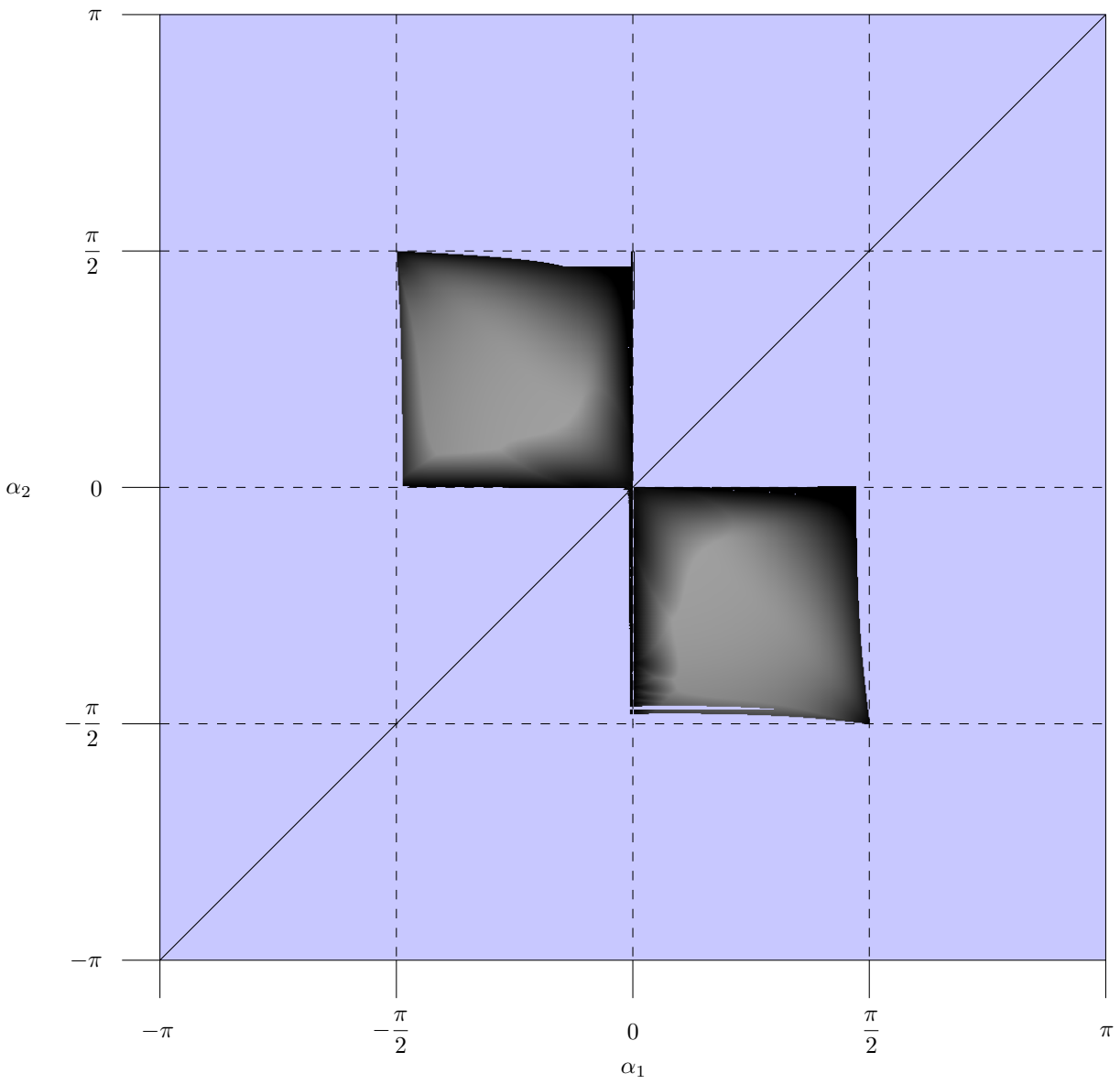

Figure 4.10: Detailed view of the slice from figure 4.9 with $\gamma = 0.5\pi$. The image is symmetric (except for numerical errors) because swapping α_1 and α_2 just creates a mirror of the frame with the same properties.

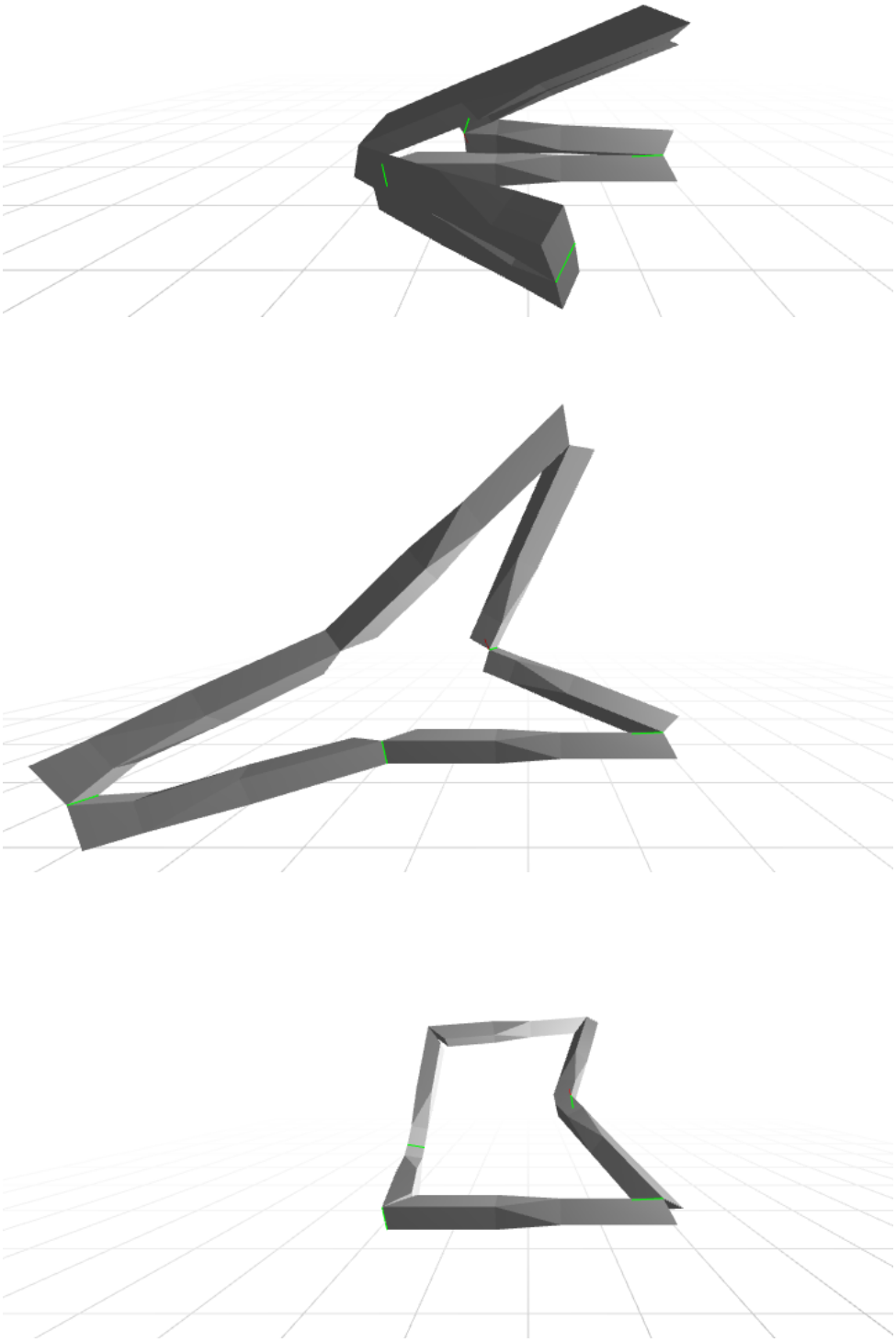

Figure 4.11: Mechanism with (approximately) the highest minimum fifth singular value as it opens.

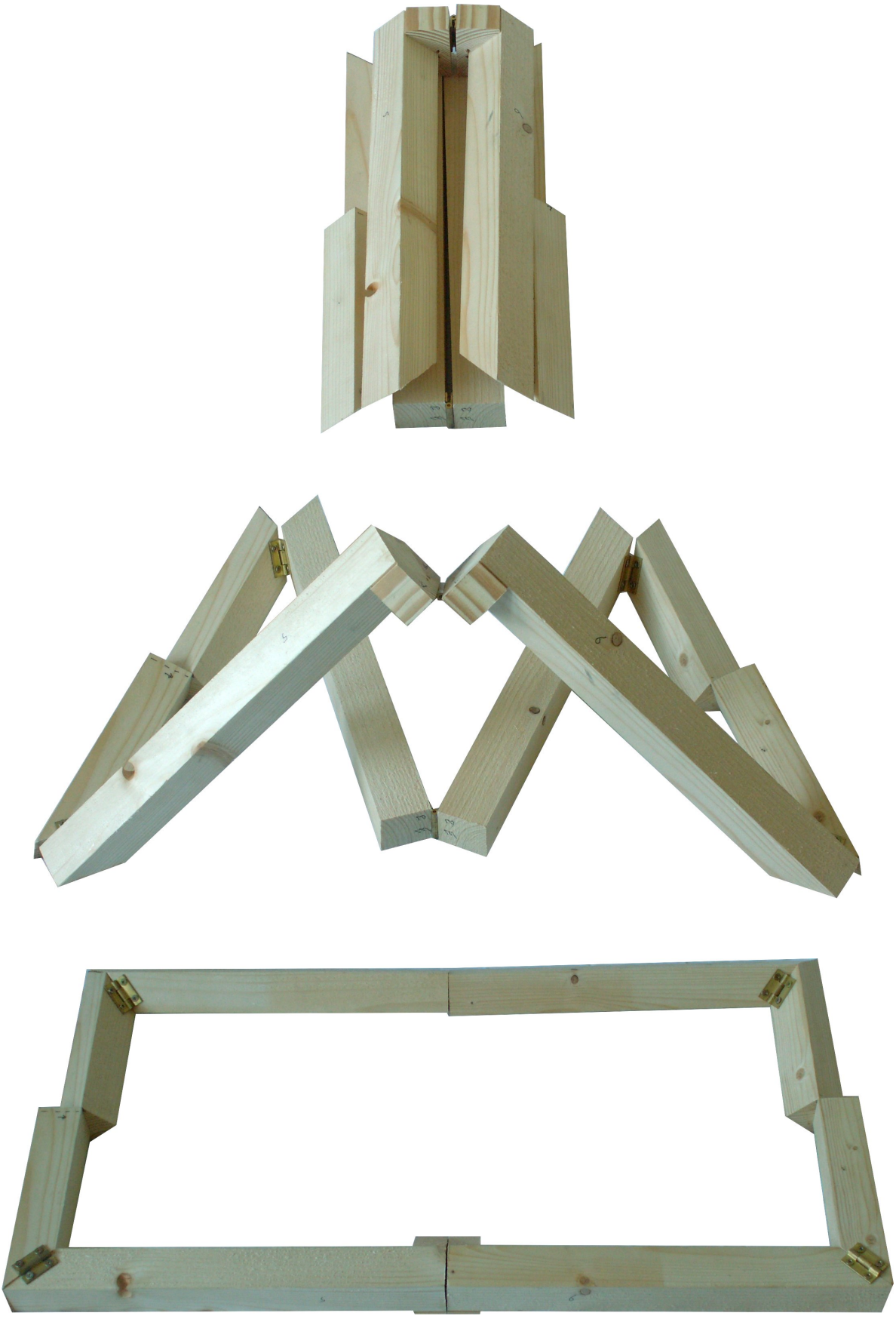

Figure 4.12: Mechanism with non-parallel end bars during deployment.

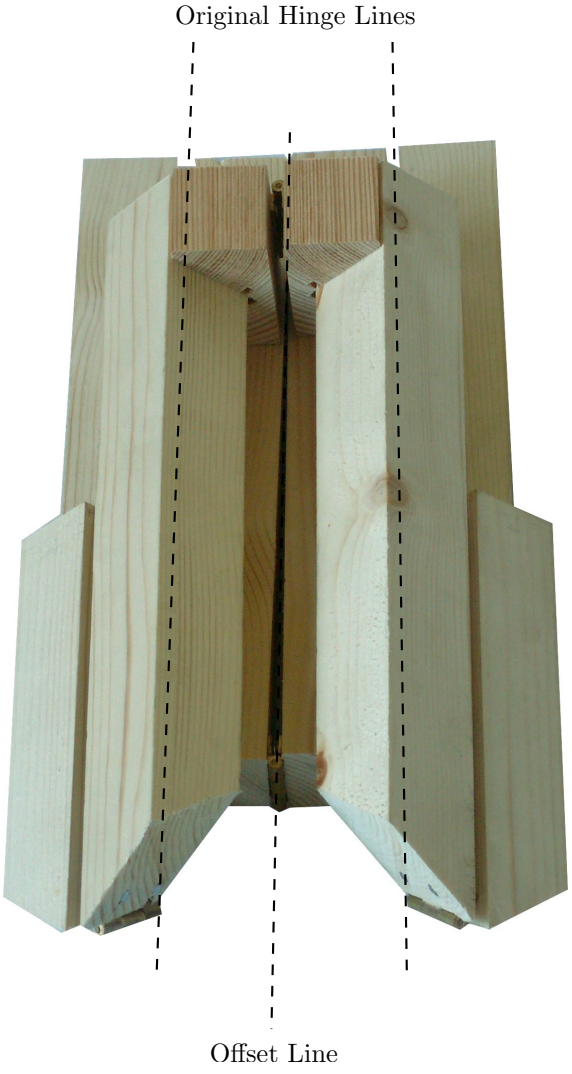

Figure 4.13: Offsetting of the symmetry hinges.

4.6 Applications and Practicalities

When building physical models of the mechanisms, several additional factors must be considered. When the mechanism is actually built it cannot be infinitely slim. In particular the two central hinges must be offset so that they are level when the mechanism is closed (figure 4.13). This has the effect of slightly changing the α_1, α_2, and γ values that give working mechanisms.

For the wooden models the choice of γ or $\gamma + \pi$ is not completely arbitrary. The incorrect choice means the mechanism must pass through itself as shown in figure 4.14.

For an antenna ring using TSR hinges, different effects would have to be considered, such as the fact that the axis of rotation changes as the hinge opens. This may actually make designing the frames easier as the hinges would be in the centre of the bars when deployed.

ideally also check that ψ_3 and ψ_4 remain in the range $[0, \pi]$.

[2]More or less - any asymmetry is a result of numerical inaccuracies.

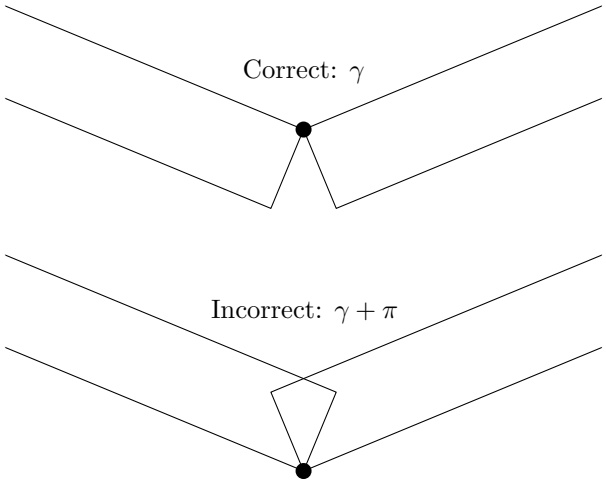

Figure 4.14: Consequences of choosing $\gamma + \pi$ instead of γ or vice versa.

As the main application envisaged is support of a SAR antenna membrane, it is important to consider how this will be attached to the frame and how it will unfold during deployment. In most mechanisms the angle between the bars goes above 90°, so the membrane would either have to stretch or be connected to the frame by stretchy ties, as with the inflatable frame (figure 1.4).

Chapter 5

Conclusions

A series of six-bar rectangular mechanisms has been found with a mobility of 1, and no kinematic bifurcations. Although the range of possibilities has not been completely explored, an empirical method for finding working rectangular frames has been described. Some mechanisms that have interesting and desirable properties will now be described.

5.1 Notable Mechanisms

5.1.1 Low Stretch

Values of roughly $\alpha_1 = -0.062\pi$, $\alpha_2 = 0.188\pi$, and $\gamma = 0.5\pi$ give a mechanism in which the angles between the side and end bars do not go much above 90°. This is useful if a membrane were attached to both bars as it would only have to stretch slightly.

5.1.2 A Sensible Mechanism

The most 'sensible' looking mechanism found was the first one, with values of $\alpha_1 = -0.25\pi$, $\alpha_2 = 0.25\pi$, and $\gamma = 0.5\pi$. These values of α_1 and α_2 also have the interesting property that varying γ from approximately 0.35π to 0.65π alters the relative orientations of the end bars as they open, with $\gamma = 0.5\pi$ keeping them parallel (see figure 5.1).

5.1.3 One Sided Opening

In most of the mechanisms one 'arm' opens by swinging underneath the mechanism, while the other folds out from the top. A small number of mechanisms (those that have the same sign of α_1 and α_2) have arms that both open on the same side, such as $\alpha_1 = 0.056\pi$, $\alpha_2 = 0.382\pi$ and $\gamma = 0.806\pi$. This property could be useful if the membrane was attached to the end bars and concertinaed.

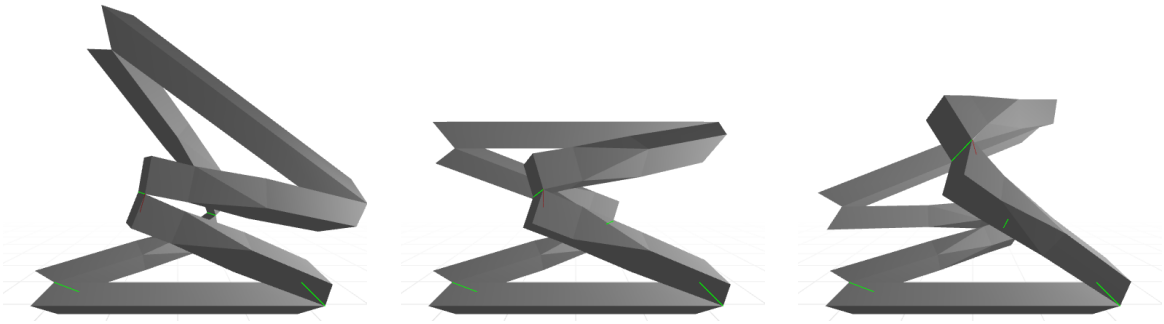

Figure 5.1: Half open mechanism with $\alpha_1 = -0.25\pi$, $\alpha_2 = 0.25\pi$, and $\gamma = 0.4\pi$ (left), $\gamma = 0.5\pi$ (centre) and $\gamma = 0.6\pi$ (right).

5.2 Future Work

The main obstacle remaining for practical use of this mechanism is the problem of how to fold the SAR or solar membrane so that it can open successfully.

It has been suggested in [12] that several frames could be linked into a larger grid. Investigation of whether this is possible for the rectangular frames described here would be useful.

This report has only been concerned with kinematics, but for use on a spacecraft it would be important to carry out a dynamic analysis of the stiffness and vibration response or a frame. This is especially important for SAR which has strict flatness and geometric consistency requirements.

As noted in [1], overconstrained mechanisms are rarely used in practice for a variety of reasons, including difficulty of design and engineers' unawareness of their existence. It seems that this is unlikely to change, and it is unclear that the mechanisms described here are significantly better than the alternative methods.

Appendix A

A Brief Introduction to Quaternions

A.1 Introduction

Quaternions are an extension of complex numbers to four dimensions, and provide an elegant alternative to using matrices to represent 3D rotations. In addition to the real and imaginary (**i**) parts of complex numbers, quaternions also have two more imaginary components (**j** and **k**). Multiplication between **i**, **j**, and **k** is not commutative, so neither is quaternion multiplication. This is a good indication that they can be used to represent rotations, as rotation is not commutative either.

The following multiplication rules apply to quaternions

$$\begin{array}{rclrclrcl} \mathbf{i}^2 & = & -1 & \mathbf{j}^2 & = & -1 & \mathbf{k}^2 & = & -1 \\ \mathbf{ij} & = & \mathbf{k} & \mathbf{jk} & = & \mathbf{i} & \mathbf{ki} & = & \mathbf{j} \\ \mathbf{ji} & = & -\mathbf{k} & \mathbf{kj} & = & -\mathbf{i} & \mathbf{ik} & = & -\mathbf{j} \end{array} \tag{A.1}$$

The last two lines are identical to vector cross products of orthogonal unit vectors which again suggests that quaternions could represent 3D constructs.

Quaternions, just like complex numbers, have a conjugate. This is given by negating the imaginary parts

$$\mathring{q} = w + x\mathbf{i} + y\mathbf{j} + z\mathbf{k} \text{ and } \mathring{q}^\star = w - x\mathbf{i} - y\mathbf{j} - z\mathbf{k} \tag{A.2}$$

The circle ($\mathring{q}$) denotes a quaternion, the star (*) indicates a conjugate.

A.2 Representing Vectors and Rotations

3D Vectors are represented by a so-called 'pure quaternion'. This is just a quaternion with a zero real component. The quaternion representation of the vector is then:

$$\begin{bmatrix} x \\ y \\ z \end{bmatrix} \longrightarrow x\mathbf{i} + y\mathbf{j} + z\mathbf{k} \tag{A.3}$$

Rotations are represented as follows. For a rotation of α about a normalised axis $[x\ y\ z]^T$ using the conventional right hand screw rule, the quaternion representation is

$$\cos\left(\frac{\alpha}{2}\right) + \sin\left(\frac{\alpha}{2}\right)(x\mathbf{i} + y\mathbf{j} + z\mathbf{k}) \tag{A.4}$$

A.3 Rotating a Vector

If a vector quaternion $\overset{\circ}{t}$ is rotated about $\overset{\circ}{r}$ (which defines both the axis and angle of rotation), then the rotated vector is

$$\overset{\circ}{t}' = \overset{\circ}{r}\,\overset{\circ}{t}\,\overset{\circ}{r}^{\star} \tag{A.5}$$

A.4 Compound Rotation

Multiple sequential rotations can be easily achieved by repeating the operation. For example, compound rotation of $\overset{\circ}{r}$ followed by $\overset{\circ}{p}$ is

$$\overset{\circ}{t}' = \overset{\circ}{p}\,\overset{\circ}{r}\,\overset{\circ}{t}\,\overset{\circ}{r}^{\star}\,\overset{\circ}{p}^{\star} = (\overset{\circ}{p}\,\overset{\circ}{r})\,\overset{\circ}{t}(\overset{\circ}{p}\,\overset{\circ}{r})^{\star} \tag{A.6}$$

Using the following property

$$(\overset{\circ}{s}\,\overset{\circ}{t})^{\star} = \overset{\circ}{t}^{\star}\,\overset{\circ}{s}^{\star} \tag{A.7}$$

A.5 Dot and Cross Products

The dot product of two vectors represented by quaternions $\overset{\circ}{t}$ and $\overset{\circ}{s}$ is given by

$$-\Re\left[\overset{\circ}{s}\,\overset{\circ}{t}\right] \tag{A.8}$$

The cross product is

$$\Im\left[\overset{\circ}{s}\,\overset{\circ}{t}\right] \tag{A.9}$$

More details about using quaternions in this way are given in [7].

Appendix B

Maxima Code

The following code was used with Maxima to find the formulae used to generate the figures 2.4 and 3.8. The first listing defines some useful functions for dealing with quaternions that are used in the succeeding listings. The final listing assumes $\beta = \alpha$.

B.1 Quaternion Initialisation

```
/* Load the atensor package. */
load(atensor);

/* Initialise it. */
init_atensor(quaternion);

/* The quaternion variables - for readability. */
i:v[1];
j:v[2];
k:v[1].v[2];

/* Function to extract the i component. Dummy is to work around a bug. */
qi(expr) := block([temp,partswitch,dummy],
partswitch:true,
if (expr = 0) then
    return(0),
temp:part(partition(expand(atensimp(expr)) + dummy, v[1]), 2),
if (temp = 0) then
    return(0),
part(partition(temp + dummy, v[2]), 1) - dummy
);

/* Conjugate function. */
qconj(expr) := block([split_i,split_j,partswitch,dummy],
partswitch:true,
if (expr = 0) then
    return(0),
split_i:partition(expand(atensimp(expr)) + dummy, v[1]),
if (part(split_i, 1) = dummy) then
    return(-part(split_i, 2)),
split_j:partition(part(split_i, 1) + dummy, v[2]),
part(split_j,1) - 2 * dummy - part(split_i,2) - part(split_j,2)
);
```

```
/* Cross Product of a and b (=imaginary(a.b)). */
qcross(a, b) := block([dummy,expr,split_i,split_j,partswitch],
partswitch:true,
expr:expand(atensimp(a.b)),
if (expr = 0) then
    return(0),
split_i:partition(expand(atensimp(expr)) + dummy, v[1]),
if (part(split_i, 1) = dummy) then
    return(part(split_i, 2)),
split_j:partition(part(split_i, 1) + dummy, v[2]),
part(split_i,2) + part(split_j,2)
);

/* Dot Product of a and b (=-real(a.b)). */
qdot(a, b) := block([dummy,expr,split_i,split_j,partswitch],
partswitch:true,
expr:expand(atensimp(a.b)),
if (expr = 0) then
    return(0),
split_i:partition(expand(atensimp(expr)) + dummy, v[1]),
if (part(split_i, 1) = dummy) then
    return(0),
split_j:partition(part(split_i, 1) + dummy, v[2]),
-(part(split_j,1) - 2 * dummy)
);
```

B.2 The Square Four-Bar Mechanism

```
/* Declare the paramaters as scalars. */

declare([psi_a, psi_b, theta, thetadash, alpha], scalar);

/* Now calculate the theta and thetadash angles. */

theta:acos(cos(atan(tan(alpha)/sqrt(2)))/sqrt(2));
thetadash:acos(-cos(atan(1/(sqrt(2).tan(alpha))))/sqrt(2));

/* Now the hinge vectors and rotations. Remember to uses . not * */

v_b:sin(thetadash) . i + cos(thetadash) . k;
r_a:cos(psi_a/4) + sin(psi_a/4) . sin(theta) . j + sin(psi_a/4) . cos(theta) . k;

/* Calculate the answer. */

v_b_rotated:atensimp(r_a.v_b.qconj(r_a));
j_rotated:atensimp(r_a.j.qconj(r_a));

/* Get the mirror plane normal and the 'hinge normal'. */

mirror_normal:atensimp(qcross(i, v_b_rotated));
hinge_normal:atensimp(qcross(j_rotated, v_b_rotated));

answer:((%pi/2) - acos(qdot(mirror_normal, hinge_normal
    / sqrt(qdot(hinge_normal, hinge_normal)
    . qdot(mirror_normal, mirror_normal)))) . 2;

answer:-ratsimp(answer);
```

```
print("Done");
```

B.3 The Square Six-Bar Mechanism

```
/* Declare the paramaters as scalars. */

declare([psi_b, theta, alpha], scalar);

/* Now calculate the theta angle. */

theta:acos(cos(atan(tan(alpha)/sqrt(2)))/sqrt(2));

/* Now the hinge vectors and rotations. Remember to use . not * */

v_a:k;
r_b:cos(psi_b/2) + sin(psi_b/2) . sin(theta) . i + sin(psi_b/2) . cos(theta) . j;

/* Calculate the rotated hinge. */

v_a_rotated:atensimp(r_b.v_a.qconj(r_b));

/* Cross it with j to get the plane normal. */

sym_plane_normal:qcross(v_a_rotated, j);
mid_hinge_vector:qcross(v_a_rotated, sym_plane_normal);

/* Normalise it. */

mid_hinge_vector:mid_hinge_vector/sqrt(qdot(mid_hinge_vector, mid_hinge_vector));

/* Now find the ab edge after rotation. */

ab_edge_rotated:atensimp(r_b.(-j).qconj(r_b));

/* Dot them, and inverse cos, * 2 gives psi_a! */

answer:acos(qdot(ab_edge_rotated, mid_hinge_vector)) . 2;

answer:ratsimp(answer);

print("Done");
```

Bibliography

[1] Y. Chen and Z. You. Curved-profile deployable structures based on bennett linkages. In *48th AIAA/ASME/ASCE/AHS/ASC Structures, Structural Dynamics, and Materials Conference*, Honolulu, Hawaii, Apr 2007. AIAA.

[2] R. F. Crawford, J. M Hedgepeth, and P. R. Preiswerk. Spoked wheels to deploy large surfaces in space: weight estimates for solar arrays., 1973. NASA-CR-2347.

[3] P. W. Fowler and S. D. Guest. A symmetry-extended mobility rule. *Mechanism and Machine Theory*, 40(9):1002–1014, Sep 2005.

[4] W. W. Gan and S. Pellegrino. Kinematic bifurcations of closed-loop deployable frames. In *Proceedings of the 5th International Conference on Computation of Shell and Spatial Structures*, Salzburg, Austria, Jun 2005. IASS/IACM.

[5] S. Guest. A family of foldable square frames., May 1999.

[6] K. Iqbal and S. Pellegrino. Bi-stable composite shells. In *Proc. 41st AIAA/ASME/ASCE/AHS/ASC Structures, Structural Dynamics and Materials Conference*, Atlanta GA, Apr 2000. AIAA.

[7] Byuing-Uk Lee. *Stereo Matching of Skull Landmarks, Appendix A: Unit Quaternion Representation of Rotation.* PhD thesis, Stanford University, 1991. Available from `http://home.ewha.ac.kr/~bulee/quaternion.pdf`.

[8] M. Leipold, H. Runge, and C. Sickenger. Large sar membrane antennas with lightweight deployable booms. 28th ESA Antenna Workshop on Space Antenna Systems and Technologies, ESA/ESTEC, May 2005.

[9] M. C. Lou, V. A. Feria, and J. Huang. Development of an inflatable space synthetic aperture radar. In *Proc. 39th AIAA/ASME/ASCE/AHS/ASC Structures, Structural Dynamics and Materials Conference*, pages 2783–2788, Long Beach, California, Apr 1998.

[10] S. Pellegrino. Large retractable appendages in spacecraft. *Journal of Spacecraft and Rockets*, 6(32):1006–1014, 1995.

[11] S. Pellegrino, C. Green, S.D. Guest, and A. Watt. Sar advanced deployable structure. Technical report, University of Cambridge Department of Engineering, Nov 2000.

[12] S. Pellegrino, S. Kukathasan, G. Tibert, and A. Watt. Small satellite deployment mechanisms. Technical report, University of Cambridge Department of Engineering, Nov 2000.

[13] Z. You and S. Pellegrino. Cable-stiffened pantographic deployable structures. part1: Triangular mast. *AIAA*, (34):813–820, 1996.